Georgia Institute of Technology

ME-4041 Computer Graphics and Computer-Aided Design

Overhead Hanging Conveyor System for Automated Manufacturing Contexts Final Report

Authors:
Calen Kirkpatrick
Sam Purdy
Brandon Hagopian

Instructor:
Dr. Yan Wang

Lab Instructors:
Casey Woodrum
Justin Yoo

April 27, 2018

Contents

1 Introduction

1.1 Situation

This project was inspired by a previous work experience by one of the contributing members. In an investment casting facility, the ceramics department was a completely automated process in which several Fanuc M-900 series robots would retrieve plates of 4-5 molds by reaching through a retractable insulating shutter from one temperature and humidity controlled area to another. With these plates of molds which weigh upwards of 800 pounds in the later stages, the robot would execute a program of dipping and depositing stucco (sand) on the exterior of the molds. After this dipping and sanding process, the plate would be returned to its temperature and humidity controlled room to dry for a certain amount of time. The conveyor would increment and the process would be started over again.

1.2 Designed Product

To serve this niche market, a modular hanging-conveyor system was devised to suit any arbitrary, but sufficiently large, temperature controlled room. To provide usefulness to this conveyor, hanger-locating devices with data collecting devices could be installed on any conveyor section, curved or straight. To satisfy the scope of this project, we focused on two main aspects of the system, how the system locates the molds in 3D space and how to collect data of the weights of the molds just prior to the robot retrieving the molds.

1.2.1 Mold Locating Improvements

Currently, the system would locate the mold in 3 dimensional space and once all the proximity sensors detect the hanger, the robot begins to retrieve the molds. However, that system currently fails due to its inability to secure the hanger in all of its rotation axises, but still activated the proximity sensors. Due to this inaccuracy, the mold is sometimes dropped by the robot, which is about a $4,000 dollar mistake. Our project tackles this issue by introducing a more flexible design that has a greater tolerance for correcting a hanger's location. This design will incorporate

profiled rollers mounted on an arm. This arm will be attached to a deployable boom, in such a way to allow for rotation, similar to devices on ski-lifts where the rollers, bearing the weight of the cable, are mounted on a branching tree-like pattern.

This arrangement, allows the roller to mate with the hanger in the location of greatest certainty. In other words, the rollers would locate the part very close to where the hanger is pinned to the rest of the chain assembly. At this location, the hanger can only vary from its nominal position by the looseness of the pinned connection, which is only fractions of an inch. That deviation is easily captured in the profile of the roller. The roller would then roll down the length of the hanger as the arms close until the point of greatest deviation from nominal is located correctly (the point farthest from the pinned connection). At this point, the proximity sensor would detect the hanger and the manufacturing process continues as it did before.

1.2.2 Data Collection Improvements

The current process also lacks any intermediate data collection, a point that this project seeks to correct. Currently, capital is invested in the mold continually without any determination if the mold remains viable. The ceramics deposition process is one of the more costly processes in investment casting due to material cost of the highly engineered slurries. Our new design would weigh the molds before every dip cycle without interrupting the robot, so that as the robot is dipping a mold, another mold will be incremented into the "Pickup" hanger gripper. That hanger would be located by the previously described system and another pneumatic piston would push on the mold, tilting the entire mold assembly to a predetermined angle (confirmed by the breakage of a laser). At the end of this piston would be a force transducer to measure the force it takes to keep the mold assembly tilted at that angle. That force would be directly proportional to mold weights, but because we are doing comparative analysis to determine the viability of the mold, that coefficient does not need to be found.

In figure 1, an example data set is given from the force transducer system previously described. Four plates of the same mold type are represented on the graph, where the green and blue data sets fall within the specified confidence interval at all times. However, the magenta data set is

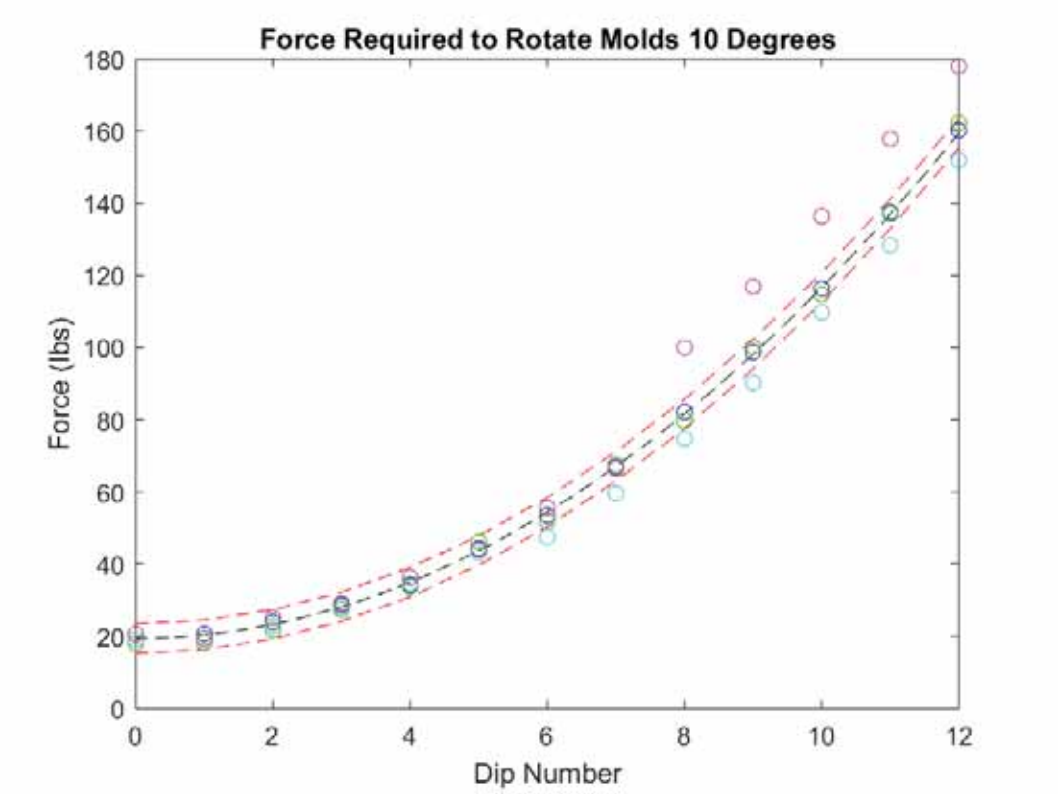

Figure 1: Example Data of the Weight Measuring System

suddenly overweight during the measuring just prior to dip #8. This could be due to the sediment in the slurries settling to the top of the slurry tank, a coarser sand type is loaded into the rainfall sander, or significant evaporation has occurred in the slurries, making them thicker. On the other hand, the cyan data set appears to be too light from dip #6 onwards, this could be due to rainfall sanders being clogged, recently added water to the slurries that haven't had time to thoroughly mix, or the slurry level is too low and doesn't wet the entire part. The goal of this project is not to fix everything that can go wrong, but to know when something does go wrong and deploy immediate corrective measures.

2 Objectives

The ultimate objective for this project is to create a modular LEGO-like system consisting of straight and curved sections of chain guides, chain tensioner, mold gripper, and a mold weighing device. The chain guide sections and tensioner can be mixed and matched to fit any shape of room. In addition, the mold grabbers can be placed anywhere along the guides to create a functional conveyor system for nearly any automated process. To be clear, this project's design implementation is created with the investment casting industry, however the system does not have any investment casting specific components, only invest casting inspiration. Therefore this system can be adapted to a variety of automated manufacturing processes.

One of the most sacred rules in manufacturing is to not cost money. Adhering to that rule, the proposed system shall not interfere with the operating robot, because the process the operating robot is conducting is a value-adding process. To respect this, the most direct method of weighing the molds of the robot take a moment to place the mold on a simple spring scale is not viable. Our design will work around this restriction by weighing the molds indirectly while they are still on the hanging conveyor.

For the design of the system, we emphasized using standard gauge materials, such as the overhead I-Beam infrastructure, plate steels, and flat bar. In order to manufacture the individual parts of the system, we only want to use a water jet cutter (for producing material-saving cutouts for resale back to material supplier), lathe (for producing the profiled contact wheels), and chop saws (for the simpler dimensioned parts). For assembly of the system, we used welding sparingly and opted for using bolts to fasten the assembly, to make the system as user serviceable as possible. As a result of this philosophy, bolted components greatly outnumber the number of welded parts.

3 Modeling

The entire assembly can be divided into 3 main subsystems, the supporting infrastructure, the hanger locating subsystem, and the mold weighing subsystem.

3.1 Supporting Infrastructure

The supporting infrastructure is defined as the structure that transfers the weight of the molds and assemblies to the surrounding building, which for the purposes of this project are assumed to be static, sufficiently strong to display negligible deflection, and be diverse enough so that our modeled system can have secured supports in any arbitrary location above the assembly.

3.1.1 Conveyor Guides

The conveyor guides are standard $5x5in$ I-Beam sections divided to fit inside manageable $4x4ft$ chunks.

i) Straight Roller Guide The modeling of the I-Beams is straightforward, starting off with the creation of the cross-section of the beam. The specific dimensions of the flanges and web was found through a metal supplier's website. After the cross-section, it was simply extruded to the desired length. This approach has the obvious advantage of being able to change only 1 parameter to change the length of the beam for other applications, such as the later described roller guide supports. Edge Blends were then used in the corners as stress relief.

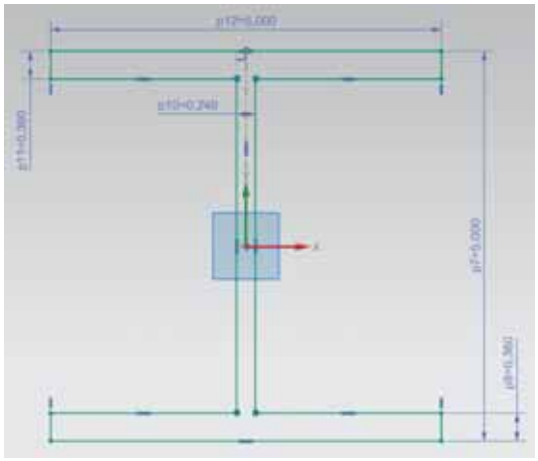

(a) Cross Section

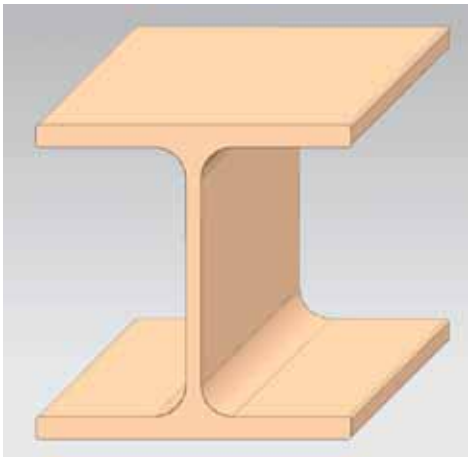

(b) Extruded Sketch to Form Solid Body

Figure 2: Modeling Steps to Form Straight I-Beam

ii) Curved Roller Guide Very similar to the straight section of the roller guide, the curved sections of the roller guides start as the same sketch, but instead of extruding in a line perpendicular to the sketch axis, the sketch is extruded along a guide using the Sweep Along Guide command. This guide sketch makes up a quarter circle, because of our previously stated goal of having a LEGO-like construction. Additional 45^o and 30^o guide sections could be made in the future to accommodate more irregular shaped rooms.

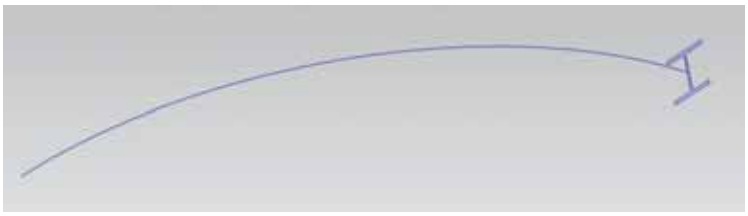

(a) Sketch of Cross Section and Guide

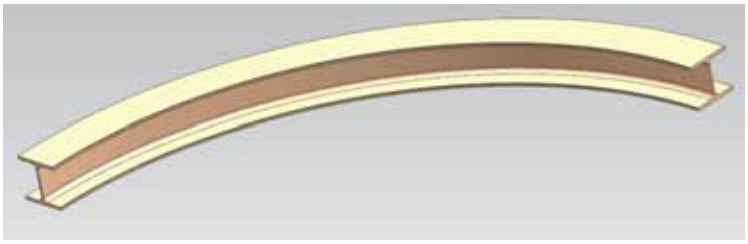

(b) Swept Along Guide to Form Solid Body

Figure 3: Modeling Steps to Form Curved I-Beam

iii) Roller Guide Support In an effort to improve the manufacturability of the design, the same standard $5x5in$ I-Beam sections were used as the supports that connect the static support structure to the fixed building surround it. The modeling process it identical to that of the Straight Roller Guide but with a different extruded length.

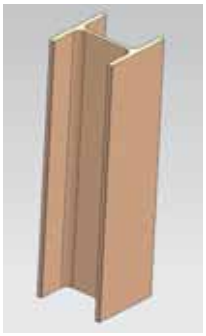

Figure 4: Extruded Sketch to Form the Support I-Beam

iv) Completed Subassembly With all of the static section of the infrastructure modeled, a completed subassembly can be made. the subassembly was made using very simple 3 "touch" mates to locate every part in 3D space relative to each other. However, to remove repetition in the assembly process, the main subassembly consists of a couple smaller subassemblies.

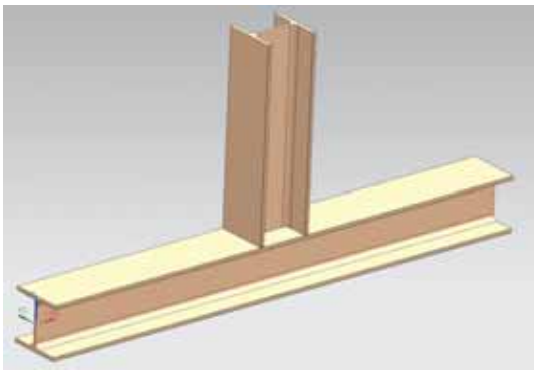

(a) Straight Section Subassembly

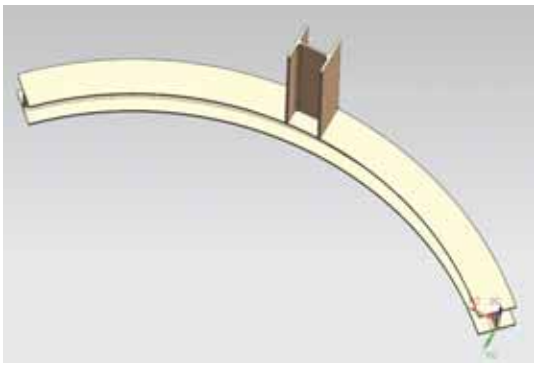

(b) Curved Section Subassembly

Figure 5: Subassemblies for the Complete Loop

The complete loop is to demonstrate the flexibility of the design to fit any sufficiently large but arbitrarily shaped room, with a combination of curved and straight sections. A straight roller guide will be shown in the future of the report in an attempt to maintain clarity. To find the number of conveyor chain links (see section 3.1.2.iii) required to saturate the design, the length of

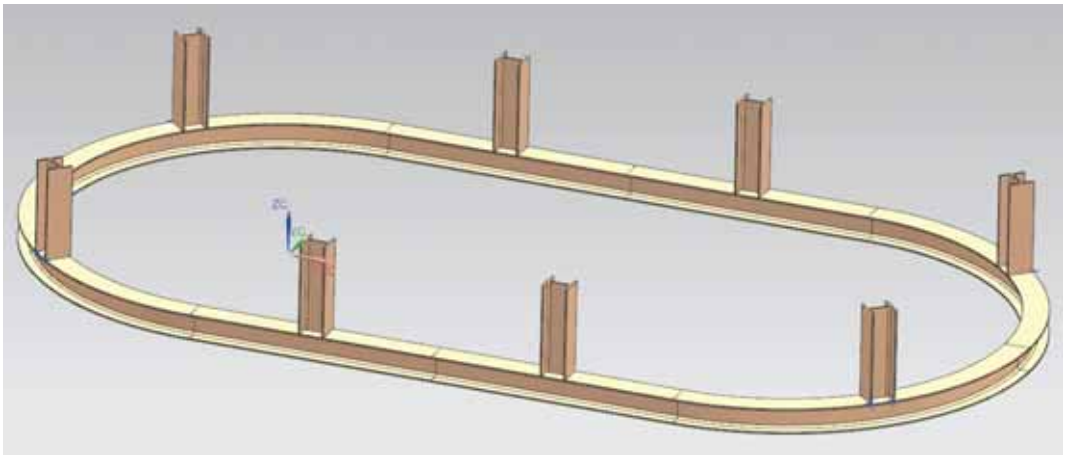

Figure 6: Complete Closed Roller Guide Loop

the track must be found and divided by the on-center distance of the chain links. The resultant would need to be rounded up to the nearest integer. The equation is as follows:

$$\#\ of\ Links = \frac{12(4S + \pi C)}{d} \tag{1}$$

Where:

$S = \#$ of Straight Guide Pieces

$C = \#$ of 90^o Curved Guide Pieces

$d =$ On-Center Distance of the Conveyor Chain Links (Inches)

3.1.2 Mobile Supporting Infrastructure

The mobile supporting infrastructure serves the purpose of moving the mold plates along the previously mentioned and modeled roller guides.

i) Guide Wheel The guide wheel rests on the roller guides and allows for relative easy moving of the entire conveyor line to allow for quick incrementing of the line. The guide wheel is created by several circular extrusions.

(a) Base Extrude (b) Rim and Central Hub (c) Central Shaft Hole Cut

Figure 7: Progression of the Guide Wheel Modeling

ii) Guide Wheel Frame The Guide Wheel Frame transfers the live load from the conveyor chain to the guide wheel above. The Wheel Frame begins where it mates with the conveyor chain and is built upwards. In figure 8(a), the frame begins as a simple rectangular extrude with the elevated sections who mate with the conveyor chain. This thickness had to be carefully determined, because two of the frames had to be inserted into the chain and then locked into place by a spacer plate. In figure 8(b), the upper extent of the extrusion is extended and trimmed to have a slanted face. On that slanted face, another extrusion was created, labeled the "Horizontal Jog Extrude". This is to make way for the I-beam flanges above the conveyor chain. At the end of this jog is a small revolve of the face to return to a vertical orientation. This process is repeated for figure e. In figure 8(f), a semicircle revolve is performed to later accept a bolt hole for the guide wheel (See section 3.1.2.i). In the next step, that bolt hole is created along with a couple of securing bolt holes on the bottom of the part. Finally figure 8(h-i) show the final result of the frame after a stress relieving edge blends and a chamfer at the bottom of the part. The chamfer is allow easier insertion of the part into the conveyor chain during assembly. Future Optimizations are made to this part in later sections (See Section 4.5).

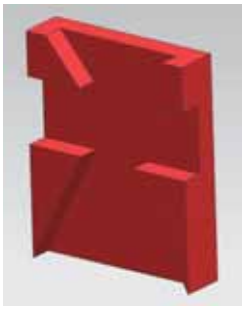

(a) Base Extrude

(b) Extrude Beginning Jog

(c) Horizontal Jog Extrude

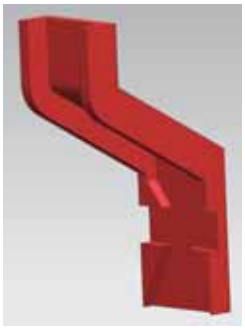

(d) Small Revolve and Extrude

(e) Horizontal Jog Back Inside

(f) Upper Wheel Mating Point

(g) Bolt Holes Established

(h) Various Edge Blends and Chamfer

(i) Reverse of Product

Figure 8: Progression of the Roller Frame

iii) Conveyor Chain The conveyor chain connects the molds together onto a continuous chain. This chain is used to separate the molds so collisions are avoided. In addition, it allows the chain of molds to move as one. This system allows for a single drive motor to be used to drive the system. The construction of the chain is similar to the previous parts where a part is extruded and then has its edges blended. For the chain though, there are two distinct components, the single link and the double link.

(a) Base Shape Extruded

(b) Edges Blended

Figure 9: Single Conveyor Chain Link

(a) Base Shape Extruded

(b) Edges Blended

Figure 10: Double Conveyor Chain Link

iv) Mold Hanger The hanger, sometimes referred to as the wishbone, is what holds the plate of molds as they are drying. It is held by a single pin at the top to act as a pivot point. This pivoting action is crucial in maintaining that the molds remain relatively vertical and are subjected to as little jerk as possible. In addition, the pin is slightly loose, this allows the molds to be located at a non-zero angle to the chain. This is useful for manufacturing settings where it is easier to

program a robot to simply swing from dropoff station to the pickup station without having to have a complex multi-axis movement. In more simple terms, the looseness allows the molds to be located in such a way that both pickup and drop off hangers are perfectly perpendicular to the robot.

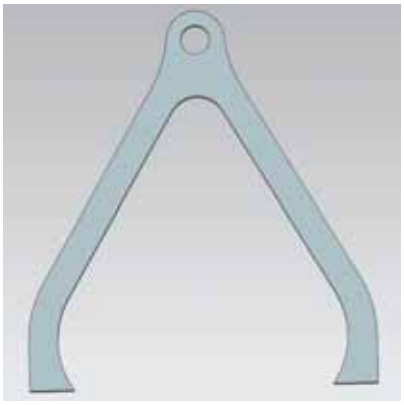

(a) Base Shape Extruded

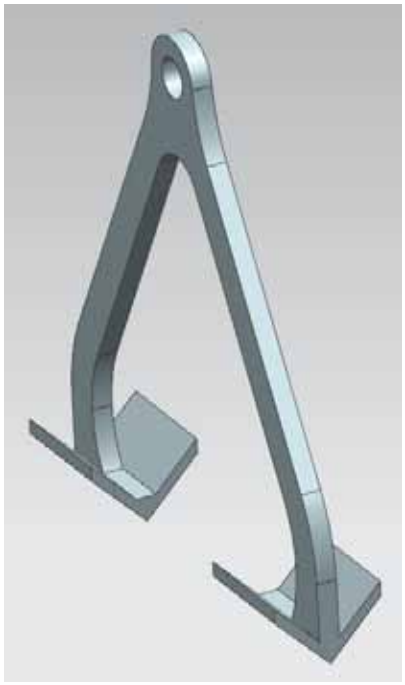

(b) T-Bar Rests Extruded and United

Figure 11: Hanger/Wishbone

v) Fasteners In this design, fasteners was preferred to connect the components together compared to welding. When using fasteners, the cost of the initial design is increase, however the long term cost of maintaining the system is reduced. Because the majority of the parts in the mobile supporting infrastructure are wear items (wheels, axles, hangers, chains), these parts need to be quickly replaceable, so we opted for a snap ring design that will be easy to replace if needed, but also preserve designed looseness in the design (See Section 3.1.2.iv).

Throughout the design, the particular parts call for different sizes of bolt diameters and lengths. For clarity, only one example bolt will be described in the modeling process as all of the design are designed in the same way.

The process to create the Bolt and snap rings is simple. The Bolt is a series of extruded circles

until the bolt head. At the bolt head, the polygon command is used to create a regular hexagon, which is then extruded. The top edge is then blended.

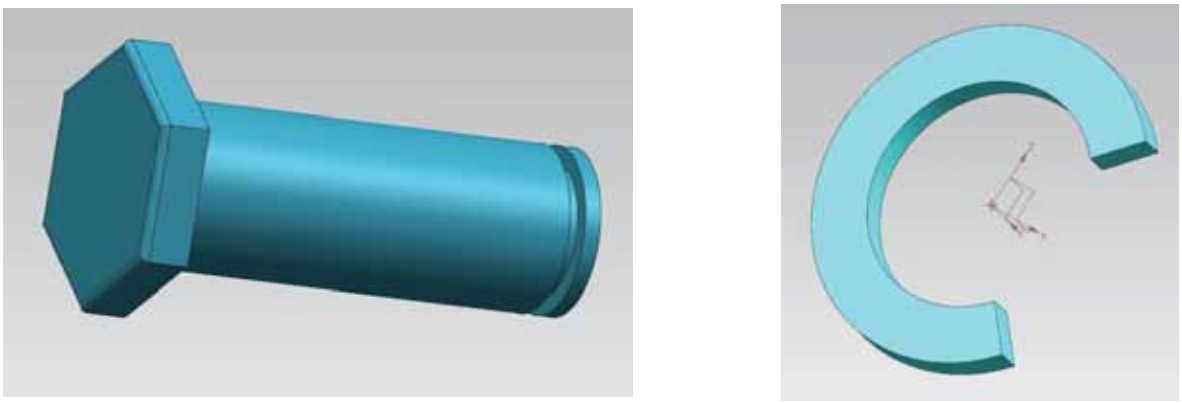

(a) Example Fastening Bolt

(b) Accompanying Snap Ring

Figure 12: Fasteners

vi) Completed Subassembly

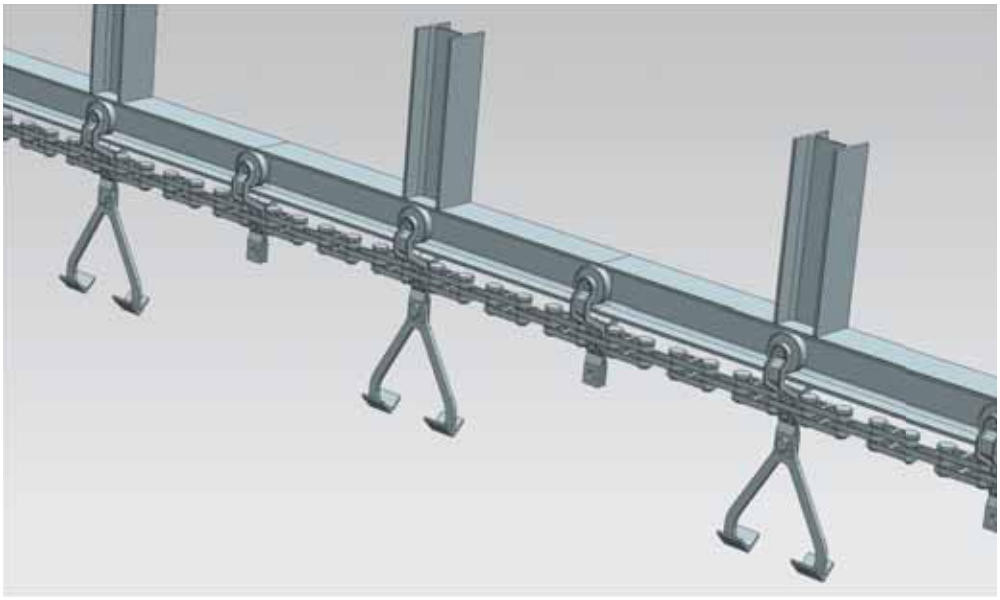

Figure 13: Completed Supporting Infrastructure Subassembly

3.2 Hanger Locating Subsystem

3.2.1 Grabbing Arm System

i) $9in$ **Piston Cylinder** The arm system needed to be able to push the arms with enough force to close around the wishbone and hold it in place. In order to provide this force, a piston cylinder was used to push a slider forward. The modeling process of this cylinder utilized a series of circular and rectangular extrudes, shown in figure 13(a-c), followed by edge blends. The tube was then hollowed out using the subtract extrude, and then the nose was added utilizing more extrudes and edge blends, shown in figure 13(d). The modeling process used here was the same as that used for the 4 inch piston cylinder.

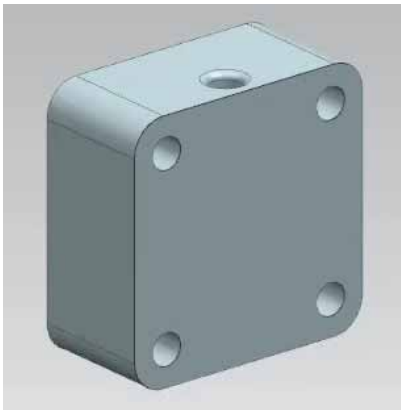

(a) Base End Extrude

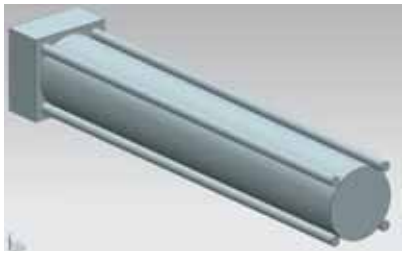

(b) Cylinder Body Extrude

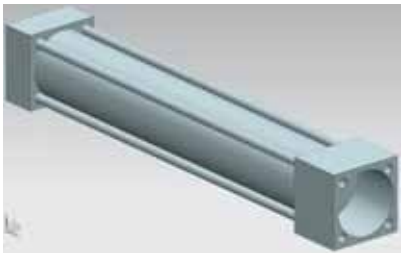

(c) Shank End Extrude and Hollowing of Cylinder Body

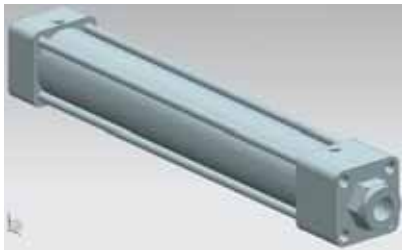

(d) Shank Hardware, Edge Blends, and Air Inputs

Figure 14: Progression of the 9in Piston Cylinder

ii) $9in$ **Piston Shank** The shank of the piston was created using an extrude to establish the rod length, shown in figure 14(a). After that, the revolve function was used to create the end along with the gaskets, as can be seen in figure 14(b). From there, more extrudes were added to

the tip of the shank and edge blends were added in order to create smooth curvature and mitigate stress concentrations. This is shown in figures 14(c-d). The modeling process presented here is identical to that used in forming the 4 inch piston shank.

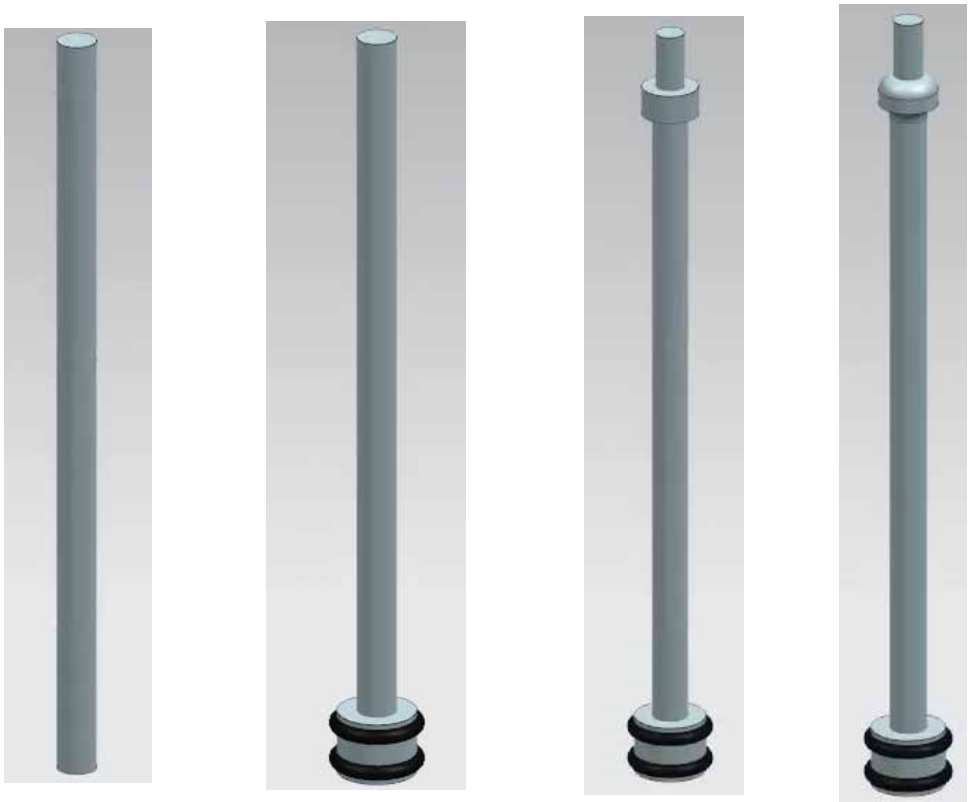

(a) Base End Extrude (b) Cylinder Piston and Seals Extruded (c) Retract Stop Extruded (d) Edge Blends Applied

Figure 15: Progression of the 9in Piston Shank

iii) $9in$ **Piston Rear Bracket** The piston is used to provide force to the grabbing arms, and as such would need to be secured by a strong set of brackets. The rear of which was produced utilizing the extrude function to create the two faces (figure 15(a)), and the subtract function to create the screw holes (figure 15(b)). The supporting angle was created by adding an extruded piece to the center of the bracket, putting a chamfer on the top corner edge, then blending the edges of the angle in order to simulate welding lines. This process can be shown in figure 15(c-d). The process depicted here is the same as that of the 4 inch piston rear bracket.

(a) Base Shape Extrude

(b) Mounting Holes Cut

(c) Reinforcing Web Extruded

(d) Web Chamfer and Edge Blends

Figure 16: Progression of the Rear Piston Bracket

iv) $9in$ **Piston Front Bracket** The second bracket that is used to secure the piston assembly is one which is able to screw into the holes of the piston cylinder, while being able to fit around the nose of the cylinder. The main body was extruded from a sketch, shown in figure 16(a). Then the gap for the nose and the screw holes was cut out using the subtract extrude function, shown in figure 16(b-c). After this the angle was added by extruding a rectangle at the center, and then adding a chamfer and edge blends, all of which can be seen in figure 16(d). This modeling process is similar to that of the 4 inch piston front bracket.

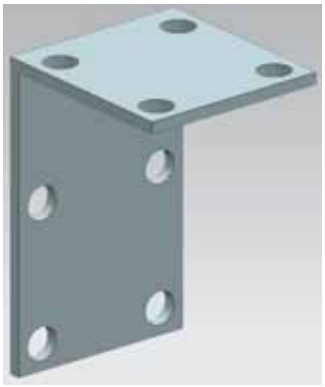

(a) Base Shape and Holes Extruded

(b) Shank Clearance Cut

(c) Reinforcing Web Extruded

(d) Web Chamfer and Edge Blends

Figure 17: Progression of the Front Piston Bracket

v) Grabber Arms The grabber arms needed to be able to reach out and hold onto the wishbone hanger. To do so it needed to leave enough room between the robot and the hanger for the weighing system to reach out and push. A rectangular cross section was extruded 18 inches, as shown in figure 17(a). Following this, another rectangular section was extruded to form the base in figure 17(b). The holes for the rotational axis and the bracket mounts were then subtracted from the body in figure 17(c). After this, the slider arm was added in order to create a way to rotate the arms, shown in figure 17(d). A pin was extruded from this arm to extend into the slider block, shown in figure 17(e). Once the geometry of the arm had been produced, edge blends were applied to every edge in order to mitigate stress concentrations, and this can be seen in figure 17(f).

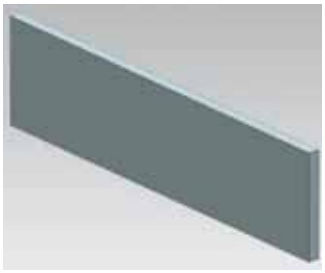

(a) Base Shape Extruded

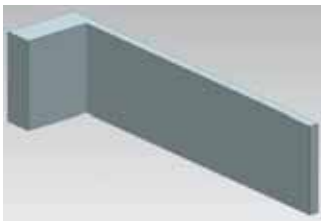

(b) Pivot Arm Extruded

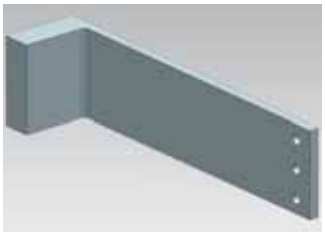

(c) Mounting Holes Cut

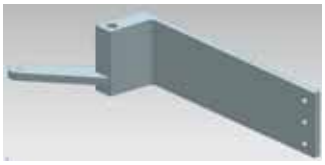

(d) Slider Block Arm Extruded

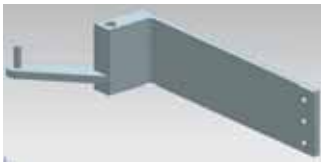

(e) Slider Block Pin Extruder

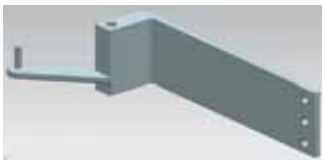

(f) Edge Blends

Figure 18: Progression of the Front Piston Bracket

vi) Slider Block The slider block needed to be able to adequately transfer force from the 9 inch piston to the grabber arms. In order to do so, the pin located on the arms needed to have adequate room to travel, such that the arm was capable of rotating 90 degrees. The range of motion could be calculated as follows:

$$\begin{aligned} \text{Angle of rotation 0: } d_x &= 6 * sin(45) = 4.24in \\ \text{Angle of rotation 45: } d_x &= 6 * sin(90) = 6in \\ \text{Angle of rotation 90: } d_x &= 6 * sin(45) = 4.24in \end{aligned} \tag{2}$$

So the maximum range of motion is approximately 1.76 inches. The size of the slider gaps then needed to be at least that long, and needed to have a width approximately equal to the diameter of the pin, to ensure as little uncertainty in the angle of the arm as possible. The block was created by extruding a rectangular shape, along with the cut-outs of the slider gaps, shown in figure 18(a). A hole was then added to the back of the block to allow the 9 inch piston to hold onto the block while pushing and pulling, shown in figure 18(b).

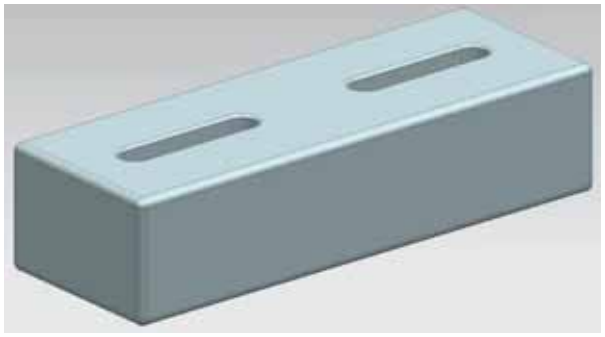

(a) Isometric View

(b) side View

Figure 19: Progression of the Slider Block

vii) Bottom Plate The bottom plate of the grabbing arm system was designed to support all of the necessary components of the system. After its initial design, shown in figure 19(a), it was decided that excess material could be saved by subtracting it from the back corners. For the final design, the basic shape of the base was extruded, and can be seen in figure 19(b). The screw holes for the all mounts were then drawn out and subtracted from the plate, shown in figure 19(c), producing the final model. The top plate was modeled using the same techniques and was adapted to inherit the same dimensions as the final design of the bottom plate.

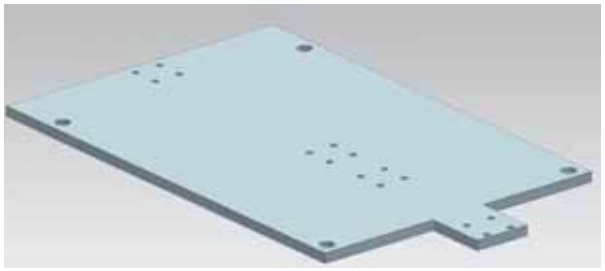

(a) Base Extrude

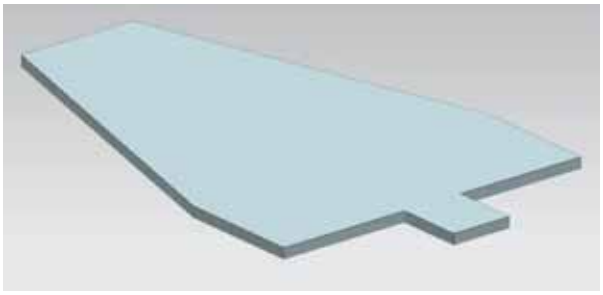

(b) Reduced Excess Material

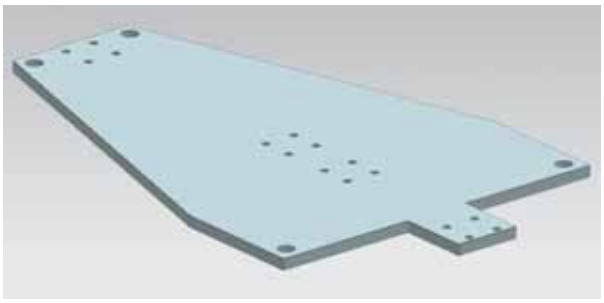

(c) side View

Figure 20: Mounting Holes Cut

viii) Plate Bolts The bolts are required to hold the top and bottom plates of the grabbing arm system together, as well as provide a rotational axis for the grabber arms. They were created using a series of extrudes along the z direction, creating separate geometries after each successive extrude. This can be seen in figure 20(a-c).

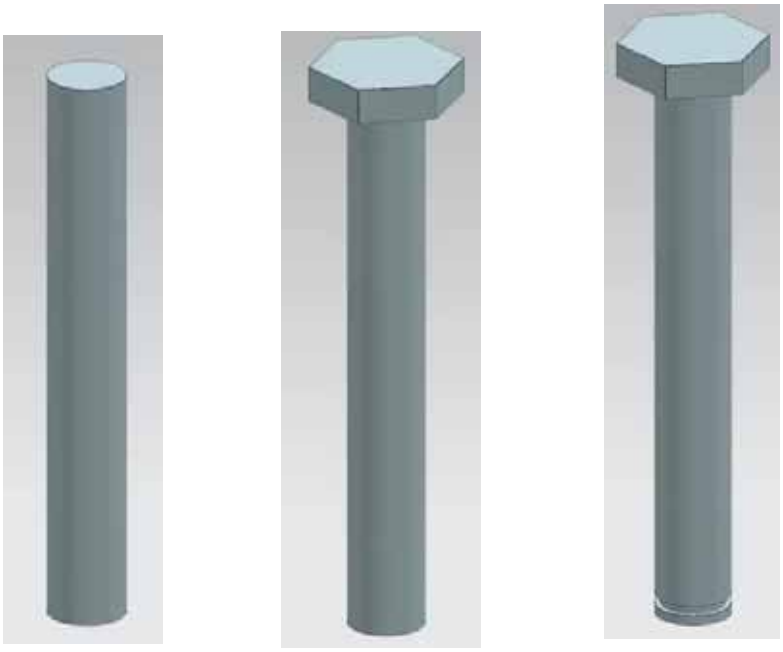

(a) Base Extrude (b) Hex Head Extruded (c) Snap Ring Trench Cut

Figure 21: Progression of the Plate Bolts

ix) Plate Bolt Snaps The bolts holding the top and bottom plates together are not threaded and therefore require a way of holding them in place aside from using nuts. The snap that was modeled allows for easy attachment and removal of the bolts, but also provides a strong attachment of the bolts. Modeling the snaps required extruding a single shape, shown in figure 21.

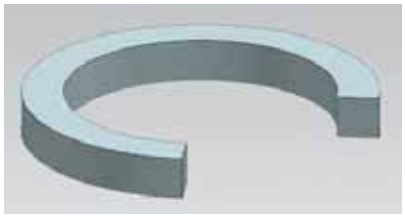

Figure 22: Snap Ring Extrude

x) Grabber Attachment The attachment was created to allow an easy way of attaching the locating bracket system the the grabbing arm system. The attachment was made using two extrudes, shown in figure 23(a), and then subtracting from them to create the screw holes for attachments, shown in figure 23(b).

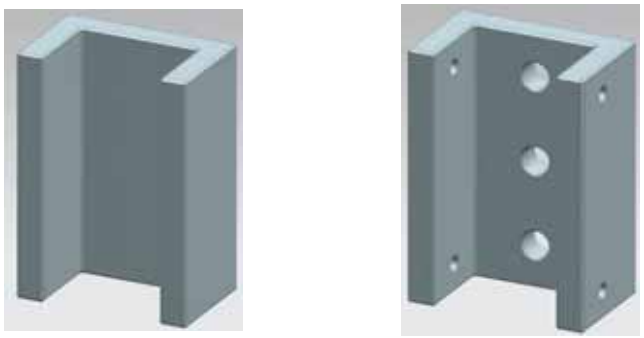

(a) Base Extrude (b) Bolt Holes Cut

Figure 23: Progression of the Grabber Attachment

xi) Completed Subassembly

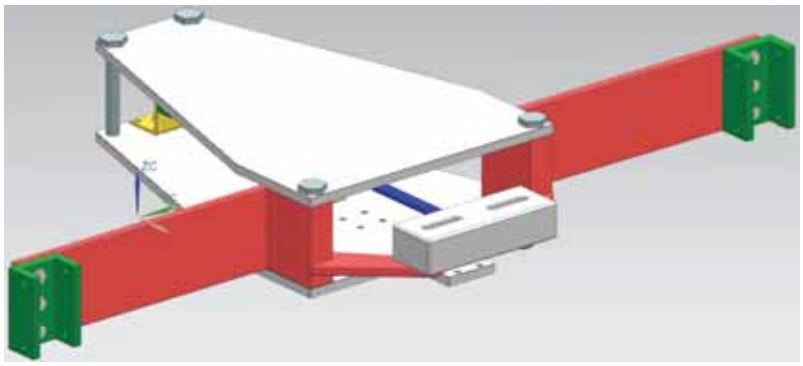

Figure 24: Grabbing Arms Retracted

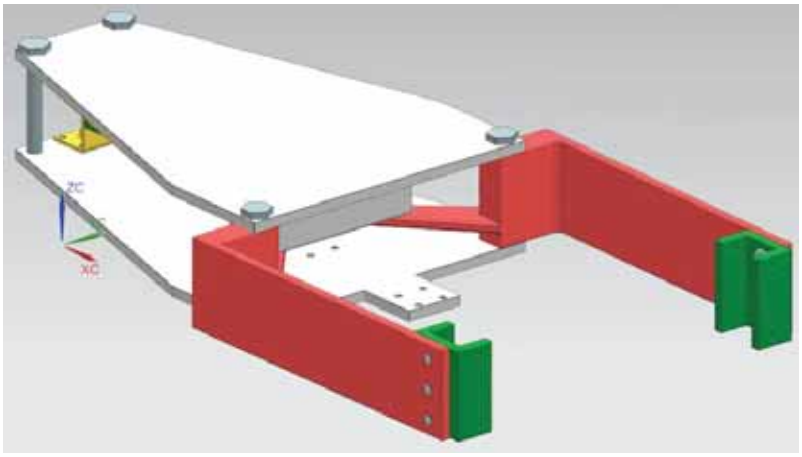

Figure 25: Grabbing Arms Deployed

3.2.2 Locating Bracket Assembly

i) Side Brackets The brackets for the locators were created to hold the entire locator system together, as well as connect to the grabber attachment piece. The method of creation for this part was simple involving a single sketch and extrude, shown in figure 26, containing all cut-outs and bolt holes for the piece. The cut-outs were added in order to eliminate excess material use.

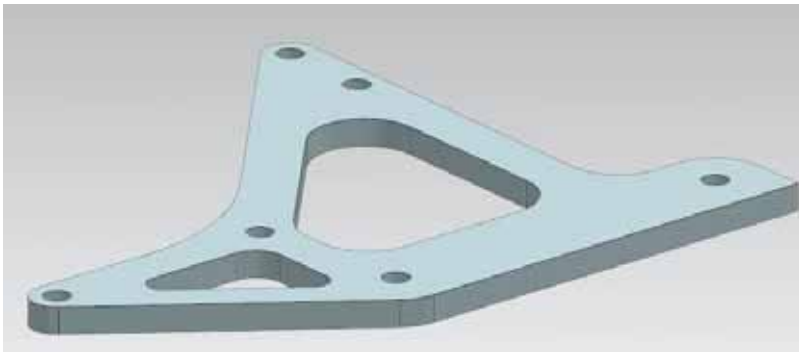

Figure 26: Side Bracket Extrude

ii) Bracket Bolts The bracket bolt was created to hold both brackets together from multiple locations. The modeling process involved extruding the body of the bolt, shown in figure 27(a), followed by the extrusion of a hexagonal shape for installment purposes, shown in figure 27(b). The modeling process for the larger bracket bolts required to mount the sub assembly to the grabber arms was the same, and for the roller bolt as well as for the induction sensor bolt, aside from a subtract to create space for the induction sensor.

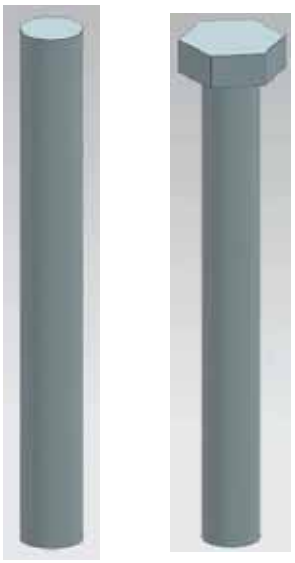

(a) Base Extrude (b) Hex Head Created

Figure 27: Progression of the Bracket Bolts

iii) Piston Rod The piston rod was modeling using an extrude for the shaft, shown in figure 28(a), as well as another for the head, shown in figure 28(b). Edge blend was then used on the head in figure 28(c) to round off the edges and reduce the amount of material used and to reduce stress concentrations.

(a) Base Extrude (b) End Effector Created (c) Edge Blends Added

Figure 28: Progression of the Piston Rod

iv) Piston Cylinder The piston cylinder was modeled using an extrude for the shaft, figure 29(a), followed by an extrude for the head, figure 29(b). Following this, a subtract extrude was used to cut out the center of the head, seen in figure 29(c), to allow for the attachment of the roller bracket. Following this, holes were subtracted out of the head to make room for attachment bolts, seen in figure 29(d), and another subtract was used to hollow out the shaft of the cylinder.

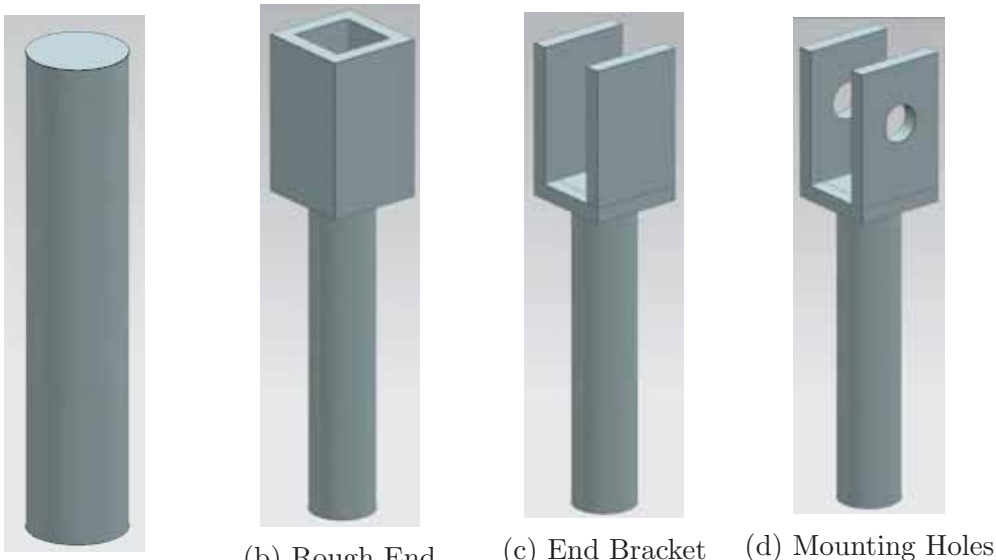

(a) Base Extrude (b) Rough End Bracket Created (c) End Bracket Shape Finished (d) Mounting Holes in Bracket Cut

Figure 29: Progression of the Piston Cylinder

v) Roller Bracket The roller bracket was modeled by extruding the basic fork shape shown in figure 30(a). Then the piston attachment was extruded and then trimmed, shown in figure 30(b-c). The holes for the wheel mounts and bolt mounts were then created using an subtract extrude, shown in figure 30(d).

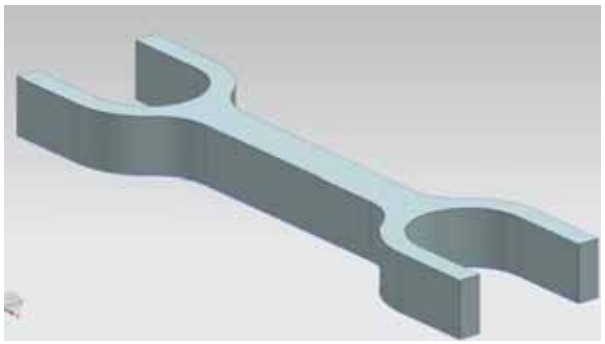

(a) Base Extrude

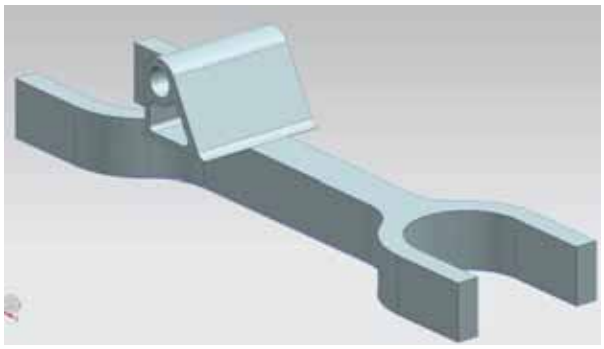

(b) Assembly Bracket Created Oversize

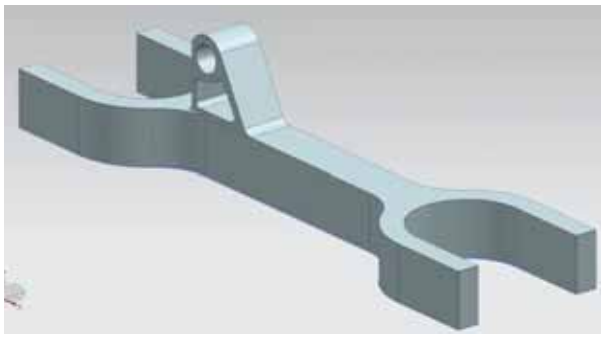

(c) Assembly Bracket Trimmed

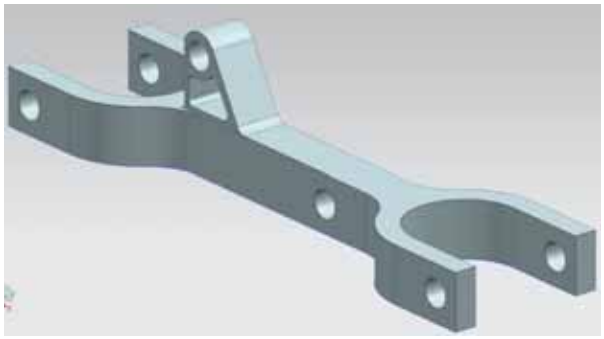

(d) Mounting Holes Cut

Figure 30: Progression of the Roller Bracket

vi) Roller Wheels The wheels were designed to allow the wishbone to slide into the center and hold on to it in order to prevent shaking during the weighing process. The center of the wheel was first extruded, show in figure 31(a). The outer portion of the wheel was then sketched and extruded twice to create the left and right side of the wheel, shown in figure 31(b). After this, a chamfer was added to the inside edges of the wheel, in order to create a surface for the wishbone to slide into place with, this can be seen in figure 31(c). Finally the center hole for the attaching bolt, in figure 31(d), was added using a subtract extrude.

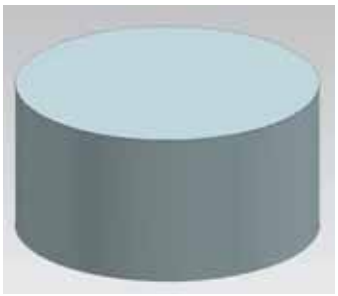

(a) Base Extrude

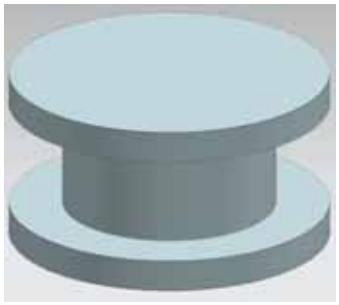

(b) Wheel Sides Created

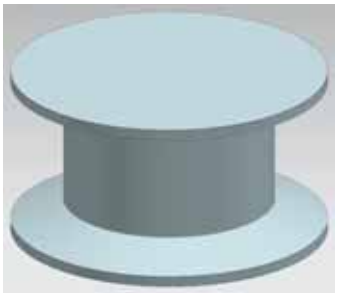

(c) Wheels Profiled

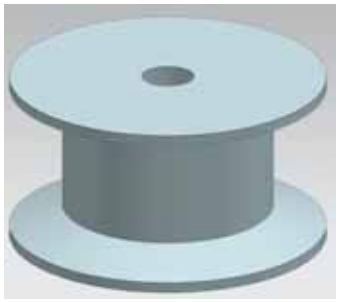

(d) Mounting Hole Cut

Figure 31: Progression of the Roller Wheels

vii) Completed Subassembly

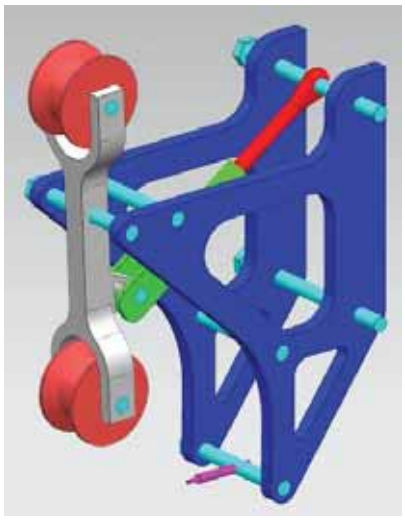

Figure 32: Locating Bracket in Starting Position (Arms Retracted)

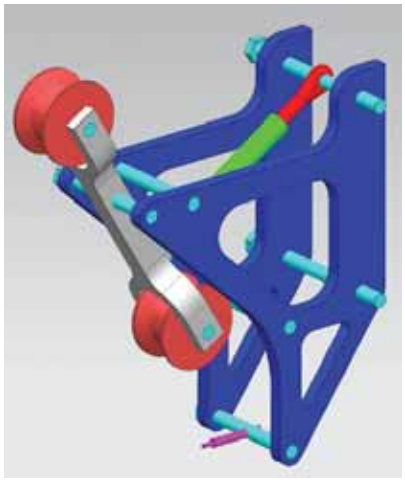

Figure 33: Locating Bracket in Final Position (Arms Deployed)

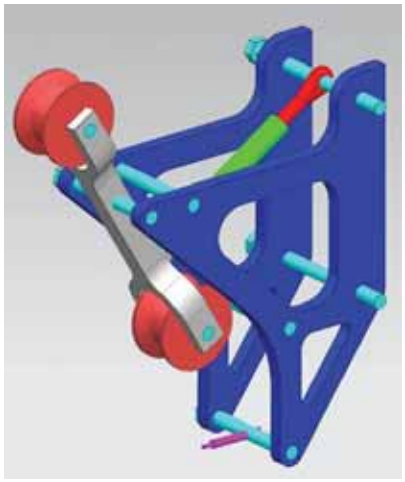

Figure 34: Locating Bracket in Final Position (Arms Deployed)

3.3 Plate Weighing Subsystem

i) $4in$ **Piston Cylinder** Identical Process to $9in$ Piston Cylinder. See Section 3.2.1.i. Main Chamber Extrusion Length was scaled down to have a $4in$ stroke.

ii) $4in$ **Piston Shank** Identical Process to $9in$ Piston Shank. See Section 3.2.1.ii. Main Length Extrusion Length was scaled down to suit the smaller cylinder stroke length. Future Optimizations are made to this part in later sections (See Section 4.3).

iii) $4in$ **Piston Rear Bracket** Identical Process to $9in$ Rear Bracket. See Section 3.2.1.iii. Minor Dimensional Changes.

iv) $4in$ **Piston Front Bracket** Identical Process to $9in$ Front Bracket. See Section 3.2.1.iv. Minor Dimensional Changes.

v) Force Transducer In order for final product to be as accurate and true to the actual design as possible, this model was borrowed with manufacturer permission. The particular product is the S-Shaped S2M Load Cell by HBM. The small form factor that measures small forces (1N to 1kN) was ideal for our purposes.

vi) U-Bracket The u bracket was created in order to ensure the T-bar hanger was properly held on to while the force transducer was able to take its measurements. The basic shape was first extruded as seen in figure 35(a). The pin that allows attachment to the force transducer was then added using another extrude, shown in figure 35(b). Then a series of edge blends were added in figure 35(c) to smooth out edges and assist in guiding the T-bar to the center of the u bracket.

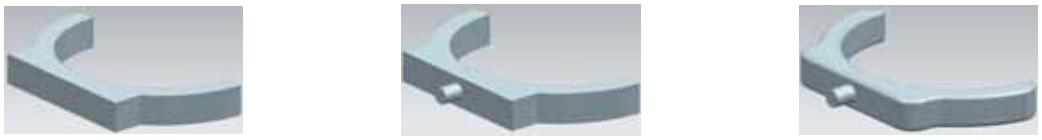

(a) Base Extrude (b) Mounting Pin Created (c) Edge Blends

Figure 35: Progression of the U-Bracket

vii) Completed Subsystem

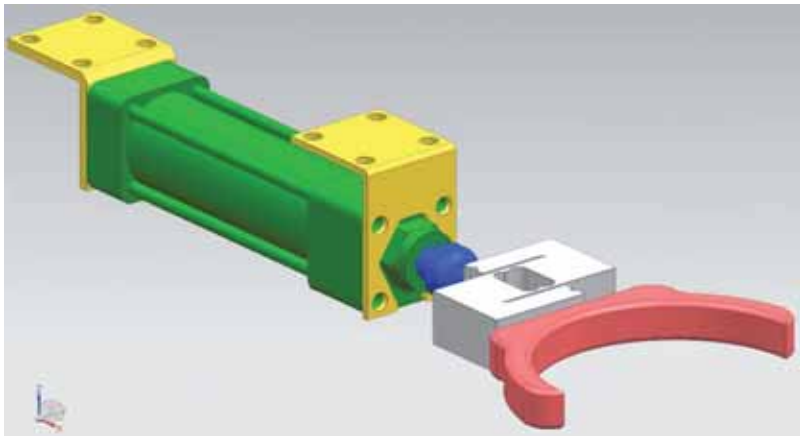

Figure 36: Plate Weighing System Retracted

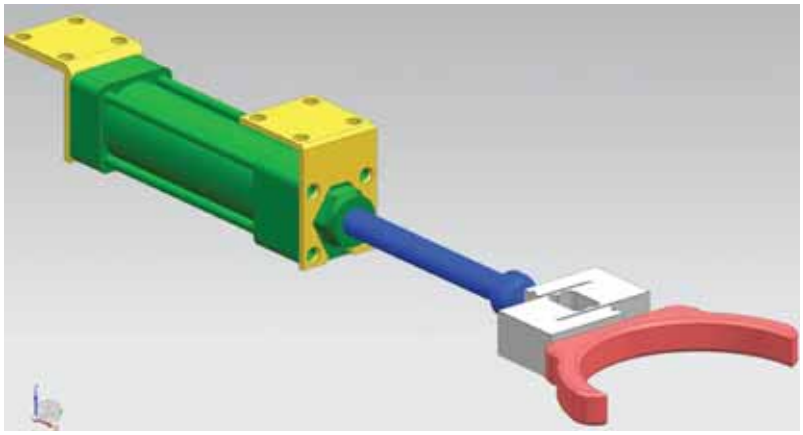

Figure 37: Plate Weighing System Extended

3.4 Mold T-Bar

The Mold T-Bar hold the molds together as a single system. This reduces the effort by the robot per mold, because more molds are processed at one time.

Using geometric constraints provided by the current manufacturing assembly, and the proposed redesign from iterating the FEA process, the basic geometric tolerances were achieved by first drawing the associated lines, and placing shapes in correct coordinates. First, a line was drawn to the correct height, and angle. Then, datum planes were used to position crucial areas of geometric changes, and also to make replicating similar sketches into different positions in space. Then, a ruled surface, revolve, and extrude were used to create surfaces in accordance to the placement of the weight measurement system, and the geometry of the Wishbone Hanger. In order to minimize stress concentrations at the extrusion where the weight of the Mold-Tree Holder is to be concentrated, a face blend was used. Lines were used with G_0 continuity to connect the top face to the lower face so a Through Curve Mesh could be used. After creating on more arc to become the bottom of the component, a Ruled Surface was used to connect the Through Curve Mesh to the bottom of the component.

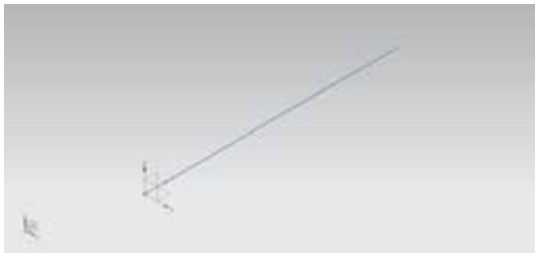

(a) Beginning Central Axis

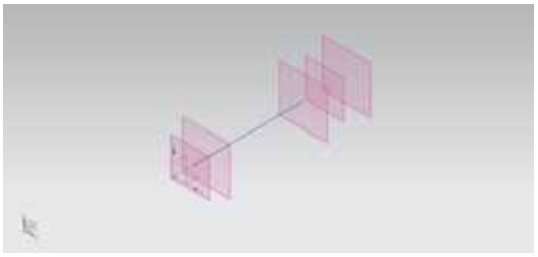

(b) Datum Planes Created

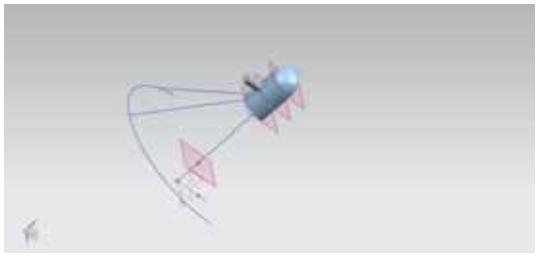

(c) Ruled Surface, Revolve, Extrude Created

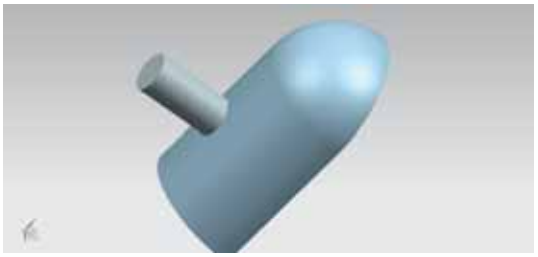

(d) Closeup of the Features

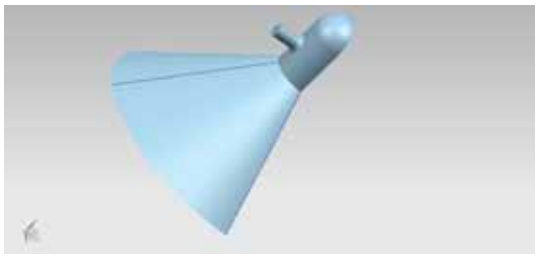

(e) Previous Extrude Blended and Through Curve Mesh Created

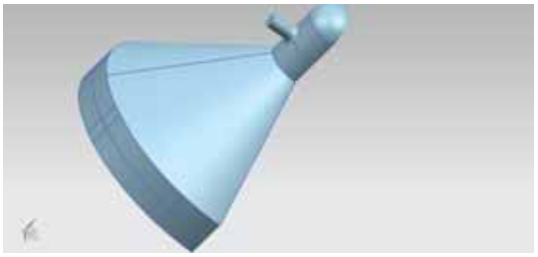

(f) Lower Ruled Surface

Figure 38: Rough Shape Defined

More Face Blends were used to minimize stress concentrations at sharp corners.For the arms that hold individual mold trees, the Sketch on Path Curve was used to define the correct normal vector in order pattern the rectangles along the face at the correct pitch, and span. Then, the Bridge Curve command was used to create tangent curves to both the face of the Through Curve Mesh, and the flat face of the Extruded Arms. The Bridge Curves were symmetrically extruded to the width of the Extruded Arms. These extruded Bridge Curves were then extruded downward through the full assembly. The excess extrude was subtracted by drawing rectangles at the exact width of the current arms. The interior leftover extrusions were trimmed away by using the Trim Body command. Edge blends were used to finalize the geometry of the hanger arms, and the shell was thickened into a solid part.

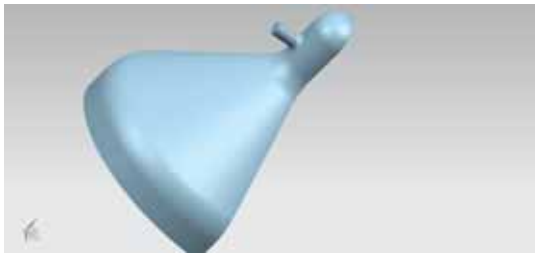

(a) Various Face Blends

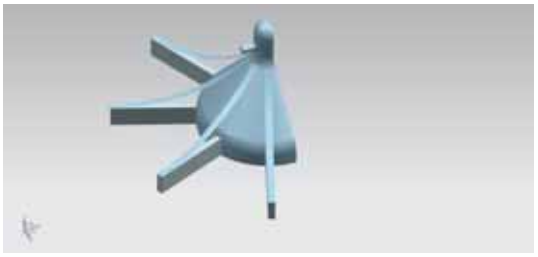

(b) Extruded Arms

(c) Bridge Curves Extruded

(d) Excess Trimmed

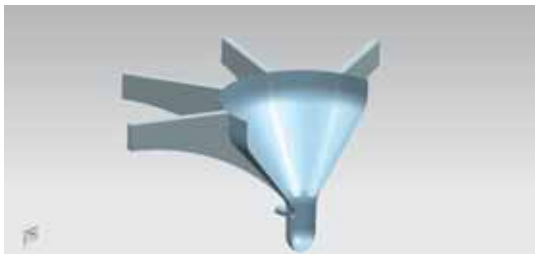

(e) Shell Thicken

(f) Final Blended Lower Section

Figure 39: Creation of Radial Arms

Because of the unsatisfactory FEA results of the first Mold-Tree Holder design, an interior geometry was sketched into the part, while also subtracting the holes for the mold trees to hang from. This sketch was extruded, then trimmed to interior curve of the component. Because of the required geometry, a previous semi-circle was copied and pasted onto datum planes and then the Through Curves command was used to create a solid body. Everything involved in the first half was copied and pasted onto a new datum, then rotated and combined with its predecessor.

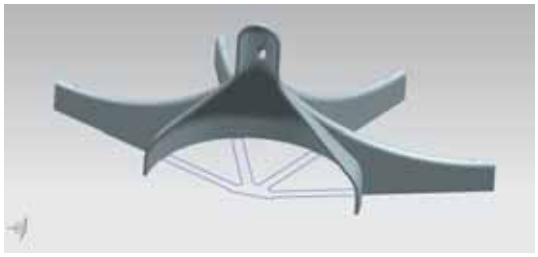

(a) Interior Feature Sketched

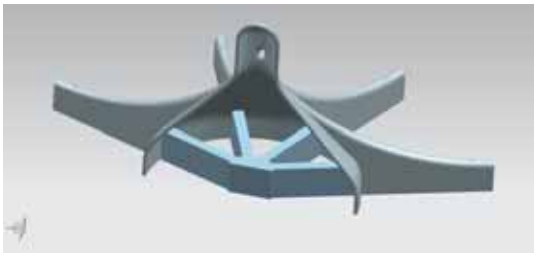

(b) Interior Support Extruded

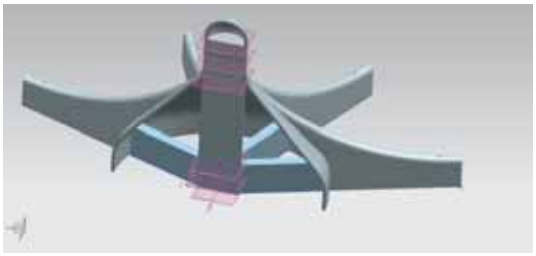

(c) Central Structure Extruded

Figure 40: Central Support Creation

After further optimization, one last component was added to reduce stress concentration at the "T" portion of the holder. First, a fourth order studio spline was drawn, connecting a .2 inch extension from the top of the holder to the edge of the circular extrude. An arc was symmetrically drawn on the edge of the circular extrude to allow for a Sweep to take place, shown here. Then the Swept surface was extruded into the body of the holder, then trimmed to fit the holder. After the sweep, the edges were blended into their surroundings.

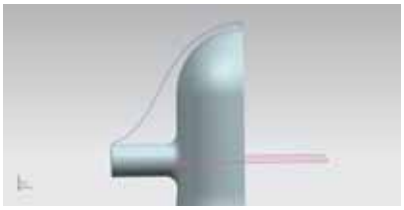

(a) Spline Sketched

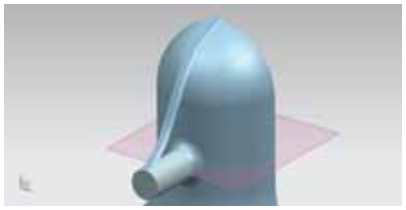

(b) Datum Created

(c) Supporting Structure Extruded

(d) Supporting Structure Blended

Figure 41: T-Section Reinforcement

(a) Front View

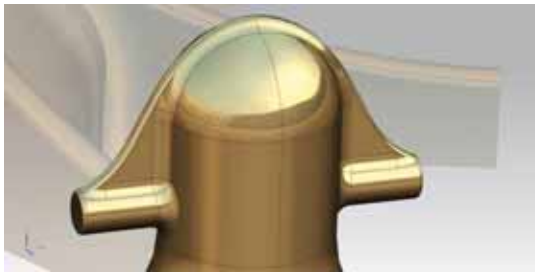

(b) T-Bar Support Close-Up

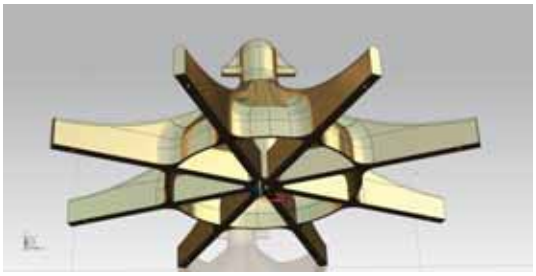

(c) Underside View

Figure 42: Completed T-Bar

3.5 Completed System

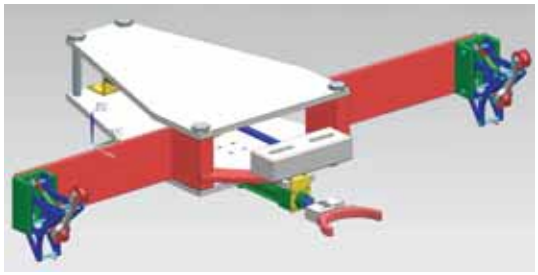

(a) System In Idle Phase

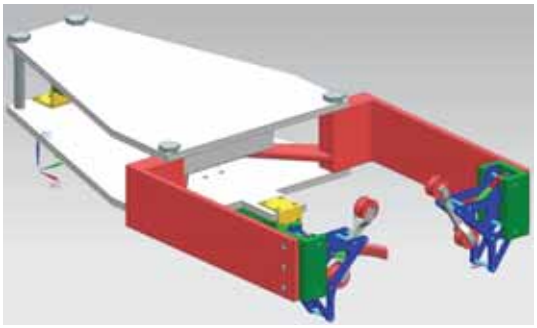

(b) System Deployed

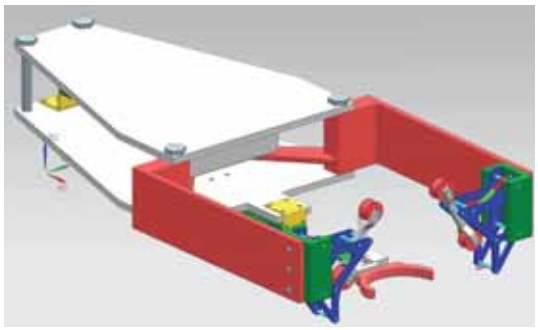

(c) Weighing System Deployed

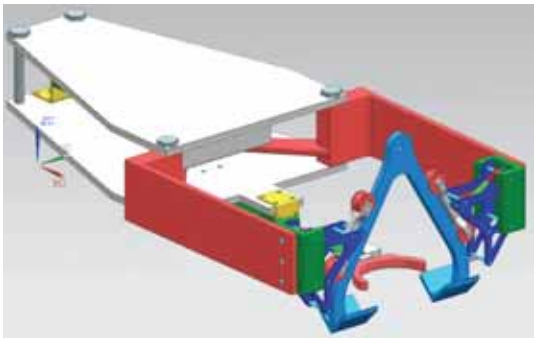

(d) Deployed System with Example Hanger

Figure 43: Completed System

4 Finite Elemental Analysis

4.1 FEA Background

4.1.1 Siemens NX FEA Background

For this project, Siemens NX was the primary software used in the structural analysis of the parts. The following FEA examples were achieved through NX's included simulation toolkit. Because the system was structurally dominated and the structural integrity of the system was the main concern (rather than thermal or acoustical loaded), the parts were solved only through NX Nastran's SOL 101 Linear Statics solution type.

4.1.2 Hand Calculation Theory Background

For verification of the Finite Elemental Analysis (FEA), a rough hand calculation was performed to verify that the displacements were believable. For these we used the following equations depending on the element type being used. The Spring Element was use to find inline displacements from inline forces, similar to how a coil spring will deform. The Beam Element will be used to determine perpendicular displacements from perpendicular forces, similar to how a diving board will deform when the diver jumps. The stiffness equations can be concatenated in the established pattern for more complex, many-node problems.

i) Spring Element 4-Node Example Equation

$$\begin{bmatrix} F_{x_1} \\ F_{x_2} \\ F_{x_3} \\ F_{x_4} \end{bmatrix} = \begin{bmatrix} k & -k & & \\ -k & 2k & -k & \\ & -k & 2k & -k \\ & & -k & k \end{bmatrix} \begin{bmatrix} d_{x_1} \\ d_{x_2} \\ d_{x_3} \\ d_{x_4} \end{bmatrix} \tag{3}$$

Where:

F = Applied and Reactionary Forces

$k = \frac{A*E}{L}$ = Spring Constant

d = Displacement

A = Cross Sectional Area of Element

E = Young's Modulus

L = Length of Element

ii) Beam Element 2-Node Example Equation

$$\begin{bmatrix} F_{y_1} \\ m_1 \\ F_{y_2} \\ m_2 \end{bmatrix} = \frac{EI}{L^3} \begin{bmatrix} 12 & 6L & -12 & 6L \\ 6L & 4L^2 & -6L & 2L^2 \\ -12 & -6L & 12 & -6L \\ 6L & 2L^2 & -6L & 4L^2 \end{bmatrix} \begin{bmatrix} d_{y_1} \\ \phi_1 \\ d_{y_2} \\ \phi_2 \end{bmatrix} \tag{4}$$

Where:

F = Applied Load and Reactionary Forces

m = Applied and Reactionary Moment Couple

d = Displacement

ϕ = Angular Displacement

E = Young's Modulus

I = Moment of Inertia of Element

L = Length of Element

4.2 Hanger Pin

Main Contributer: Sam Purdy

4.2.1 Definitions

The chosen design for our project involved the load hanging on a wishbone-shaped hanger, and this wishbone is attached to the Hanger System via a single bolt, so that the Wishbone was still capable of rotating. As such, with the heavy loads that will be added to the wishbone, the bolt needed to be able to withstand large shearing forces without fracturing due to high stress concentrations. Our original design for this bolt was a 1 in diameter steel bolt, that had a contact area with the Wishbone and Wishbone Brackets that in total is 1.1 in long. The material this would be made out of was chosen to be AISI 4340 Steel ($E = 2.799 * 10^7$ psi) due to its high strength and rigidity, and due to the size of each bolt, this would also be relatively inexpensive to use throughout the system. Through research and previous experience with similar systems, the maximum load on the Wishbone is assumed to be ≈ 1000 lbs (i.e. the load transferred from the wishbone to the bolt is also 1000 lbs). Through many trials of bolts with different diameters, the design was changed in order to keep the amount of material used to a minimum, while still being able to keep our desired factor of safety. Due to the stresses built up in other parts, a diameter less than 0.5 in was not an option. The results of these trials based on finite element analysis are presented in Table 1, where the only dimensions that were changed were the diameters, the lengths must remain the same due to system constraints.

Diameter (in)	Max Displacement (in)	Max Stress (psi)	Safety Factor
1	$3.6096 * 10^{-5}$	$18,474$	9.25
0.75	$5.8461 * 10^{-5}$	$30,753$	5.56
0.6	$4.6833 * 10^{-5}$	$25,018$	6.83
0.5	$7.1590 * 10^{-5}$	$35,308$	4.83

Table 1: Displacements and Stresses for Different Bolt Sizes

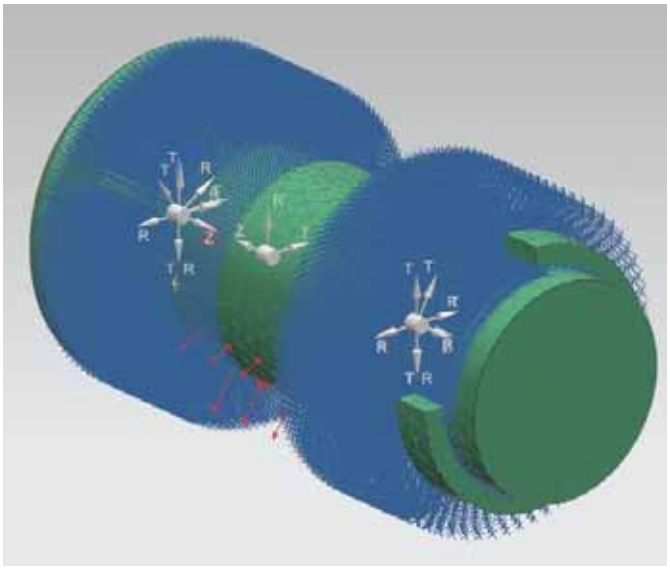

Figure 44: Mesh View of Bolt and Applied Loads and Constraints

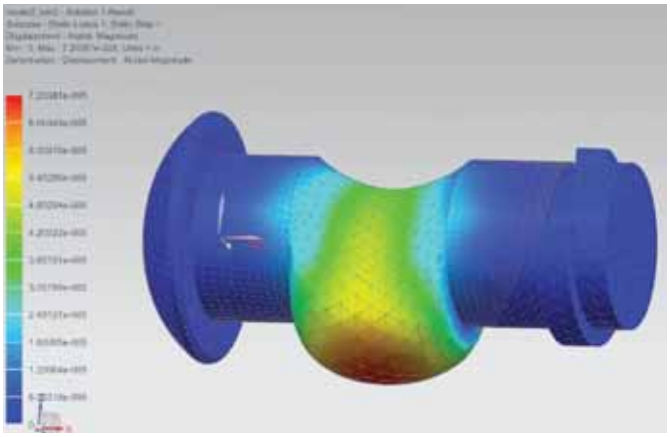

Figure 45: Bolt Displacement Due to Shearing Load

4.2.2 FEA Using NX

In order to perform FEA analysis on the bolt, we utilized the NX NASTRAN application. The bolt was run through several iterations before approaching the final design. The outer portions of the bolt were constrained using a pin constraint, and a bearing load of 1000 *lbs* was applied to the center portion, as seen in Figure 44. A mesh size of 0.05 *in* was used to analyze the part. Figure 45 is shown below, depicting an exaggeration of the displacement of the bolt.

Here the maximum displacement of any node is computed to be $7.2 * 10^{-5}$ *in* and the maximum stress of any node is $35,308$ *psi*. Further analysis with a hand calculation is necessary to determine if the results of the FEA are reliable.

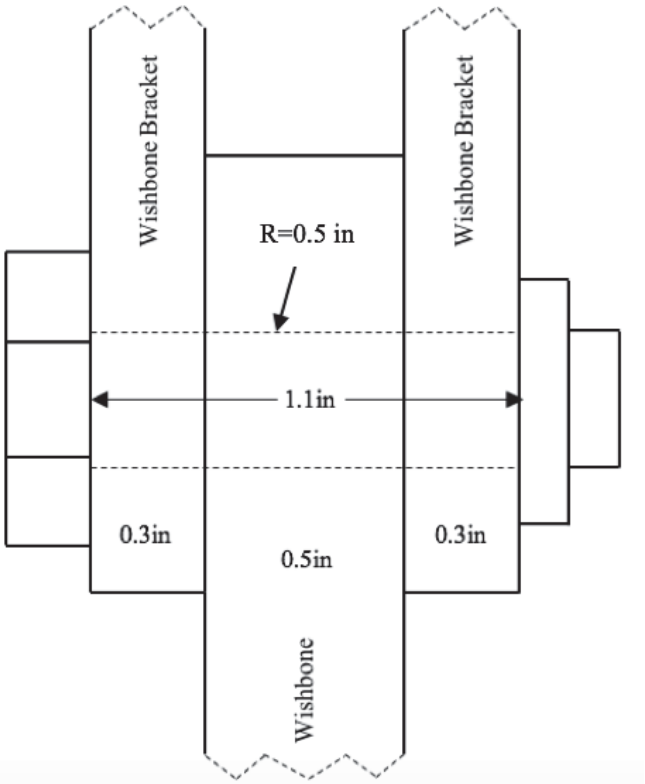

Figure 46: wishbone Bolt Side View, with Dimensions

4.2.3 Verification

In order to simplify the problem, the two ends of the bolt, shown in Figure 46, were taken away and the new faces that were created were assumed to be fixed.

By breaking up the bolt into seven nodes as shown in Figure 47, a relatively close estimate of the displacement and angles of each node due to the load were able to be calculated by assuming the system to be a simple beam problem. With 1000 *lbs* loaded downward across the central 0.5 *in* from the Wishbone, there would logically be a 500 *lbs* reaction across the remaining 0.3 *in* on each side due to the Wishbone Brackets. The distribution of forces at each of the nodes is then shown in Figure 48. As it is laid out, with the reaction forces of the Wishbone Brackets already assumed, this prevents the fixed ends from creating their own reaction forces, which could cause an error in the estimate.

As is shown, the bolt was split into seven nodes, with unequal spacing in the middle and at the ends. Distributing the nodes as such allowed for the assumed distribution of weight to be closer to

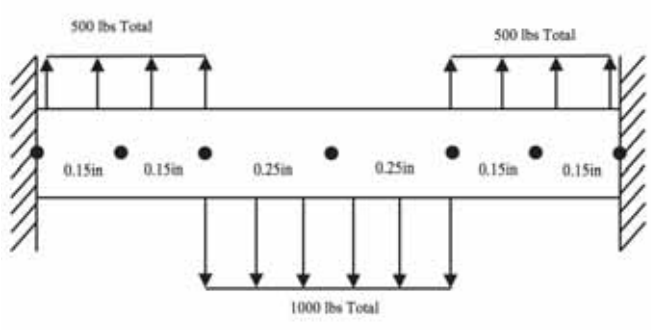

Figure 47: Node Layout for the Wishbone Bolt Simplification

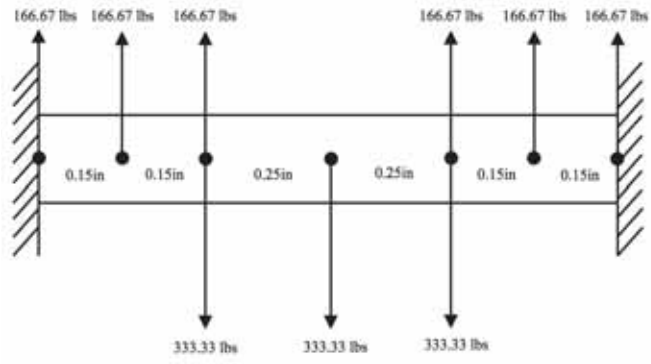

Figure 48: Node Layout with Forces Distributed to Respective Nodes

the real distribution. Next the stiffness matrix, $\left[k\right]$, needed to be set up, and can be seen below in Equation 1.

$$
\left[k\right] = EI * \begin{bmatrix}
12L_1^{-3} & 6L_1^{-2} & -12L_1^{-3} & 6L_1^{-2} & & & & & & & & \\
6L_1^{-2} & 4L_1^{-1} & -6L_1^{-2} & 2L_1^{-1} & & & & & & & & \\
-12L_1^{-2} & -6L_1^{-2} & 24L_1^{-3} & 0 & -12L_1^{-3} & 6L_1^{-2} & & & & & & \\
6L_1^{-2} & 2L_1^{-1} & 0 & 8L_1^{-1} & -6L_1^{-2} & 2L_1^{-1} & & & & & & \\
 & & & & \begin{matrix}-12L_1^{-3} \\ \\ \end{matrix} & \begin{matrix}-6L_1^{-2} \\ \begin{pmatrix} 12L_1^{-3} \\ +12L_2^{-3} \end{pmatrix} \end{matrix} & \begin{matrix} \\ \begin{pmatrix} 6L_1^{-2} \\ +6L_2^{-2} \end{pmatrix} \end{matrix} & -12L_2^{-3} & 6L_2^{-2} & & & \\
 & & & & \begin{matrix}6L_1^{-2} \\ \\ \end{matrix} & \begin{matrix}2L_1^{-1} \\ \begin{pmatrix} -6L_1^{-2} \\ +6L_2^{-2} \end{pmatrix} \end{matrix} & \begin{matrix} \\ \begin{pmatrix} 4L_1^{-1} \\ +4L_2^{-1} \end{pmatrix} \end{matrix} & -6L_2^{-2} & 2L_2^{-1} & & & \\
 & & & & -12L_2^{-3} & -6L_2^{-2} & 24L_2^{-3} & 0 & -12L_2^{-3} & 6L_2^{-2} & & \\
 & & & & 6L_2^{-2} & 2L_2^{-1} & 0 & 8L_2^{-1} & -6L_2^{-2} & 2L_2^{-1} & & \\
 & & & & & & -12L_2^{-3} & -6L_2^{-2} & \begin{matrix}12L_2^{-3} \\ +12L_1^{-3}\end{matrix} & \begin{matrix}-6L_2^{-2} \\ +6L_1^{-2}\end{matrix} & -12L_1^{-3} & 6L_1^{-2} \\
 & & & & & & 6L_2^{-2} & 2L_2^{-1} & \begin{matrix}-6L_2^{-2} \\ +6L_1^{-2}\end{matrix} & \begin{matrix}4L_2^{-1} \\ +4L_1^{-1}\end{matrix} & -6L_1^{-2} & 2L_1^{-1} \\
 & & & & & & & & -12L_1^{-3} & -6L_1^{-2} & 24L_1^{-3} & 0 & -12L_1^{-3} & 6L_1^{-2} \\
 & & & & & & & & 6L_1^{-2} & 2L_1^{-1} & 0 & 8L_1^{-1} & -6L_1^{-2} & 2L_1^{-1} \\
 & & & & & & & & & & -12L_1^{-3} & -6L_1^{-2} & 12L_1^{-3} & -6L_1^{-2} \\
 & & & & & & & & & & 6L_1^{-2} & 2L_1^{-1} & -6L_1^{-2} & 4L_1^{-1}
\end{bmatrix}
$$

From here the Force and Displacement equality could be drawn up in the form shown in

Equation 2.

$$\begin{bmatrix} F_{1_y} \\ M_1 \\ F_{2_y} \\ M_2 \\ F_{3_y} \\ M_3 \\ F_{4_y} \\ M_4 \\ F_{5_y} \\ M_5 \\ F_{6_y} \\ M_6 \\ F_{7_y} \\ M_7 \end{bmatrix} = \begin{bmatrix} k \end{bmatrix} \begin{bmatrix} d_{1_y} \\ \phi_1 \\ d_{2_y} \\ \phi_2 \\ d_{3_y} \\ \phi_3 \\ d_{4_y} \\ \phi_4 \\ d_{5_y} \\ \phi_5 \\ d_{6_y} \\ \phi_6 \\ d_{7_y} \\ \phi_7 \end{bmatrix}$$

Now, we know all of the forces applied, but we will assume that F_{3_y} and F_{5_y} aren't known in order to help the equation solve. Each of the forces is shown in Figure 48. We also know that all of the moments are 0 because there are no applied moments. The only two displacements that are known were assumed to be 0, and those are d_{1_y} and d_{7_y}. For the stiffness matrix, we also know that $E = 27.99x10^6\ psi$, $I = \frac{\pi D^4}{64} = 0.01227\ in^4$, and $L_1 = 0.15\ in$ and $L_2 = 0.25\ in$. Plugging all of our knowns into the equation and solving for the unknowns gives us the following answers:

$$\begin{bmatrix} d_{1_y} \\ \phi_1 \\ d_{2_y} \\ \phi_2 \\ d_{3_y} \\ \phi_3 \\ d_{4_y} \\ \phi_4 \\ d_{5_y} \\ \phi_5 \\ d_{6_y} \\ \phi_6 \\ d_{7_y} \\ \phi_7 \end{bmatrix} = \begin{bmatrix} 0\ in \\ -9.70 * 10^{-5} \\ -1.43 * 10^{-5}\ in \\ -9.16 * 10^{-5} \\ -2.67 * 10^{-5}\ in \\ -6.97 * 10^{-5} \\ -3.60 * 10^{-5}\ in \\ -3.04 * 10^{-14} \\ -2.67 * 10^{-5}\ in \\ 6.97 * 10^{-5} \\ -1.43 * 10^{-5}\ in \\ 9.16 * 10^{-5} \\ 0\ in \\ 9.70 * 10^{-5} \end{bmatrix} \qquad \begin{bmatrix} F_{1_y} \\ M_1 \\ F_{2_y} \\ M_2 \\ F_{3_y} \\ M_3 \\ F_{4_y} \\ M_4 \\ F_{5_y} \\ M_5 \\ F_{6_y} \\ M_6 \\ F_{7_y} \\ M_7 \end{bmatrix} = \begin{bmatrix} 166.67\ lbs \\ 0\ lbs * in \\ 166.67\ lbs \\ 0\ lbs * in \\ -166.67\ lbs \\ 0\ lbs * in \\ 333.33\ lbs \\ 0\ lbs * in \\ -166.67\ lbs \\ 0\ lbs * in \\ 166.67\ lbs \\ 0\ lbs * in \\ 166.67\ lbs \\ 0\ lbs * in \end{bmatrix} \tag{5}$$

Most notably we can see that the calculated forces at nodes 4 and 5 agree with the ones shown in Figure 48, so this confirms there were no errors in the calculation. Also, we see that the maximum displacement calculated was $3.60 * 10^{-5}\ in$ at the center node, which makes sense that it would have the most movement due to symmetry. From the FEA shown earlier, the computed displacement was $7.2 * 10^{-5}\ in$. The calculated displacement is not even off by a factor of two, so we can say that the results given from NX are reliable. The only potential reasons for this difference are from the fact that the piece is not 2D and the end nodes are not truly fixed. The interaction of nodes along the outside of the bolt have interactions that could cause the bolt to deform differently than a theoretical beam element.

4.3 Weight Measuring Piston Shank

Main Contributer: Calen Kirkpatrick

4.3.1 Definitions

For this assignment, the shank of a pneumatic cylinder will be analyzed. The objective of this analysis is to see if the deflection of the beam will be significant enough to risk breaking of the seal in the neck of the cylinder. Rubber seals at the end of the cylinder separate the highly machined interior of the cylinder and the gritty, messy exterior. If that neck seal is compromised, dirt could reach the interior rubber seals that separate the high pressure and low pressure chambers. If the deflection of the beam compromises that seal, maintenance will be increased and with bad seals, the force exerted will be lessened due to escaping gas from the cylinder housing.

If the deflection is deemed significant enough to endanger the seal, a guide will be designed and placed. This guide will be designed in such a way to bear the vertical force so the cylinder shank does not, in an effort to prolong life and maintain accuracy in data collection.

The pneumatic cylinder's documentation from the manufacturer states the shanks are "high tensile ground and polished hard chrome plated steel piston rod", therefore we will assume the material properties to be similar to 4340 Steel.

Because of the previously assumed material of the component, we will use the material properties of 4340 Steel specified in Siemens NX. The material properties from that database are as follows:

$$Young's\ Modulus = E = 193\ MPa = 2.799 * 10^7\ psi$$

$$Poisson's\ Ratio = \nu = 0.284$$

$$Yield\ Strength = 470\ MPa = 68,168\ psi$$

For the forces, the maximum anticipated load on the system is 1000 lbs. With some trigonometry and knowledge of levers, we determine that the horizontal component exerted on the shank of the pneumatic cylinder is 200 lbs and a vertical component of about 35 pounds. Generously

converting these values to metric, we receive the following loads:

$$F_x = 200\ lbs \approx 1,000\ N$$

$$F_y = 35\ lbs \approx 160\ N$$

4.3.2 Original Design

The original design of the shank is how it was presented to the consumer from the manufacturer. A simple half inch shank with a screw at the end of the shank. That screw will mate with the force transducer. However, the force transducer will be difficult to simulate because of its unknown internal structure. However, being significantly shorter, thicker cross section, and with the manufacturer's statement that it exhibits "minimal deflection", we will ignore the force transducer in this analysis.

The shank itself will be assumed to be fully extended with a length of 4 inches out of the cylinder ($2L$). The interior of the shank will also be modeled, extending 2 inches into the cylinder casing (L). With this setup, we will have 4 nodes with equal length of L between them in the system for our later hand calculated verification. The shank will be supported in two places, at the neck of the pneumatic cylinder and by the interior. The interior will support the shank fully because of its wider body and contact with the pneumatic cylinder's sides and top, but the neck will only support perpendicular forces to the axis of the shank and will not resist any rotation.

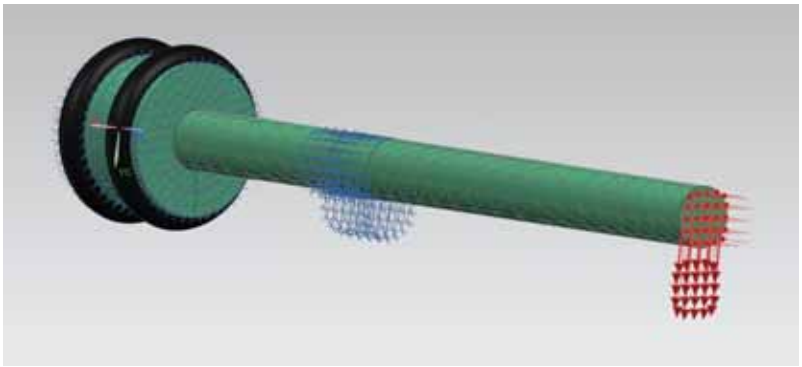

Figure 49: Constraints and Loads in Siemens NX

Not only is the displacement manageable at around a hundredth of an inch (therefore a guide is unnecessary), the Von Misses strength of the shank shows the member is under stressed. Aiming

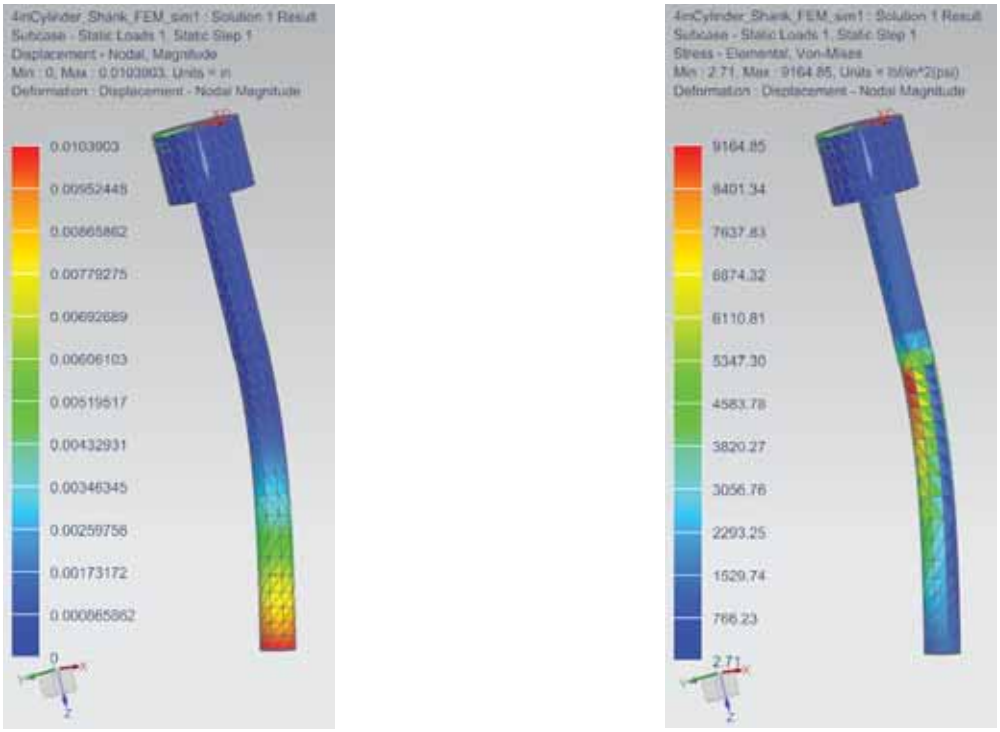

(a) Displacement (b) Von Misses Stress

Figure 50: Finite Elemental Analysis Results of Original Design

for a Factor of Safety of about 3, the shank appears to be too strong for our use case. If the weight of the shank is reduced by machining the sides, the pneumatics for the system will be able to drive the weight measuring assembly, more quickly, reducing the time it will take to get a reading. The faster we complete the process, the more time the plate has time to settle before the robot interacts with it. However to be clear, the settling action should only be a backup, these specific pneumatic cylinders were chosen because of their cushioning feature, where they would only release pressure at a given rate, similar to a flow restrictor valve.

4.3.3 Iteration #1

To match our Factor of Safety more closely to our desired value, reduction of the shaft's cross sectional area is required. A milling operation could easily achieve this goal. The complementary piston seal on the cylinder body would be replaced to match this operation. Perfect matching of the cylinder body and shank is less important on this end of the cylinder so an imperfect seal from a "rough" milling operation is acceptable, as this space is only used to retract the shank back,

rather than exert a specified amount of force. In addition, the neck of the cylinder will have a rubber seal to hold the pressure.

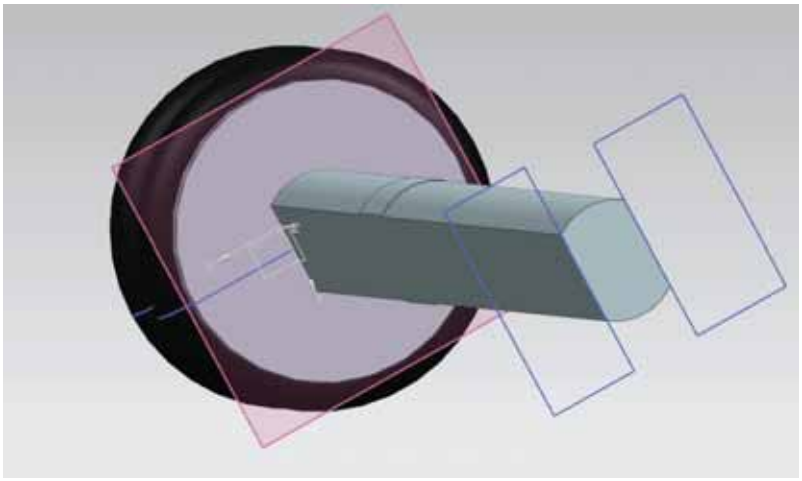

Figure 51: Modification of the Shank

For this iteration, the original 0.5in diameter shaft is milled down to $0.3in$ across the flats. The other hardware (U-Bracket) will be mounted and secured on the end of the shank so that the "long" dimension of the shank will resist the bending caused by F_y.

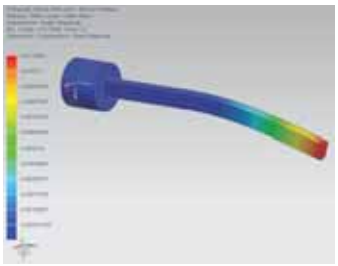

(a) Displacement

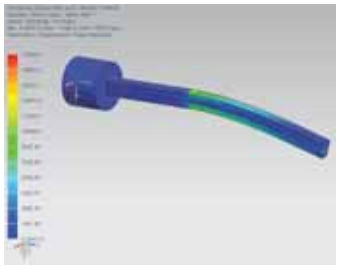

(b) Von Misses Stress

Figure 52: Finite Elemental Analysis Results of Iteration #1

The Factor of Safety remains too high. A greater reduction in material will not harm performance of the piston, but will allow it to be more responsive when taking the weight measurements due to having less inertia.

4.3.4 Iteration #2

The across flats dimension will be reduced further to $0.2in$

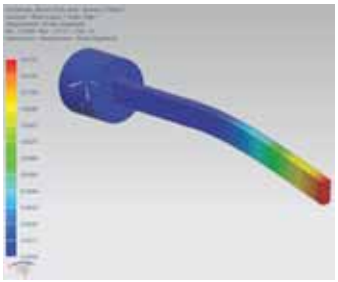

(a) Displacement

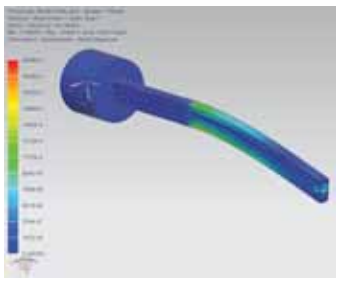

(b) Von Misses Stress

Figure 53: Finite Elemental Analysis Results of Iteration #2

Distance Across Flats (in)	Max Displacement (in)	Max Stress (psi)	Safety Factor
0.5	0.0104	9,165	7.44
0.3	0.0110	17,294	3.94
0.2	0.0131	22,464	3.03

Table 2: Displacements and Stresses for Different Shaft Thicknesses

The Maximum Von Misses Stress has reached about 1/3 of the yield strength of the material and deflection remains acceptable.

However, the thickness of the shank has become quite thin. Buckling may present a problem to the structural integrity of the beam. If buckling does present a formidable risk, the milling operation across the sides of the beam may need to be altered, such as forming a cross pattern or using a ball nose mill to create a shape somewhat reminiscent of an I-beam.

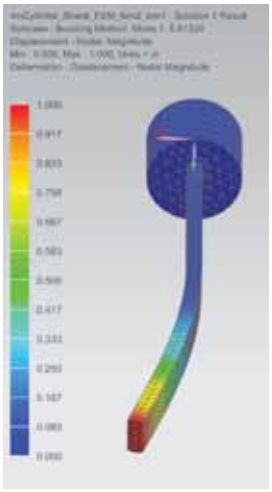

Figure 54: Linear Buckling Analysis on Thinned Shank

The first load case of the buckling analysis is shown above. With an eigenvalue of over 5

and a yielding factor of safety of 3, buckling will not present a risk. If overloaded, the shank will yield instead of buckling. Although workers are not expected to near the machine when operating, due to the proximity to heavy automated machinery like the central 6-axis Robot, it is important to note that a yielding failure is more desirable compared to a sudden buckling failure. A sideways buckling failure as shown in the figure above may throw objects in unanticipated directions, potentially causing bodily harm. On the contrary, a yielding structure, will fail fairly unspectacularly in a safe direction (downwards because of the downwards F_y force).

4.3.5 Verification

Because of our modifications to the shank, the cross section will be assumed to be a rectangle of dimensions $0.45 * 0.2$ in. The slight undersizing of the "long" dimension will produce an upper limit of stress and displacement of the shank. With this steel's density of $7,850\ \frac{kg}{m^3}$, the linear mass (λ) of this steel rod will be $0.4558\ \frac{kg}{m}$. In addition, the equation for the moment of inertia will be calculated as being $\frac{1}{12}m(w^2 + h^2)$. With these values, we can determine the following properties:

$$L = 2\ in = 0.0508\ m$$

$$Cross\ Sectional\ Area = A = 5.8 * 10^{-5}\ m^2$$

$$Spring\ Constant = k = \frac{A * E}{L} = 4.4443 * 10^8\ \frac{N}{m}$$

$$Beam\ Stiffness\ Constant = \frac{E * I}{L^3} = 2.2060 * 10^8\ \frac{Nkg}{m^3}$$

i) Spring Element Solution

$$\begin{bmatrix} F_{x_1} \\ F_{x_2} \\ F_{x_3} \\ F_{x_4} \end{bmatrix} = \begin{bmatrix} k & -k & & \\ -k & 2k & -k & \\ & -k & 2k & -k \\ & & -k & k \end{bmatrix} \begin{bmatrix} d_{x_1} \\ d_{x_2} \\ d_{x_3} \\ d_{x_4} \end{bmatrix}$$

$$\begin{bmatrix} F_{x_1} \\ 0 \\ 0 \\ 1000N \end{bmatrix} = \begin{bmatrix} k & -k & & \\ -k & 2k & -k & \\ & -k & 2k & -k \\ & & -k & k \end{bmatrix} \begin{bmatrix} 0 \\ d_{x_2} \\ d_{x_3} \\ d_{x_4} \end{bmatrix}$$

$$\begin{bmatrix} 0 \\ 0 \\ 1000N \end{bmatrix} = \begin{bmatrix} 2k & -k & \\ -k & 2k & -k \\ & -k & k \end{bmatrix} \begin{bmatrix} d_{x_2} \\ d_{x_3} \\ d_{x_4} \end{bmatrix}$$

$$\begin{bmatrix} d_{x_2} \\ d_{x_3} \\ d_{x_4} \end{bmatrix} = \begin{bmatrix} 0.00000453\ m \\ 0.00000907\ m \\ 0.00001360\ m \end{bmatrix} = \begin{bmatrix} 0.0001785\ in \\ 0.0003569\ in \\ 0.0005354\ in \end{bmatrix} \tag{6}$$

The data from both sources look good and believable. The spring deflection was expected to be much lower than the overall displacement shown in Siemens NX. The displacements grow as they move farther from the neck of the beam which also indicates a good calculation.

ii) Beam Element Solution

$$\begin{bmatrix} F_{y_1} \\ m_1 \\ F_{y_2} \\ m_2 \\ F_{y_3} \\ m_3 \\ F_{y_4} \\ m_4 \end{bmatrix} = \frac{EI}{L^3} \begin{bmatrix} 12 & 6L & -12 & 6L & & & & \\ 6L & 4L^2 & -6L & 2L^2 & & & & \\ -12 & -6L & 12+12 & -6L+6L & -12 & 6L & & \\ 6L & 2L^2 & -6L+6L & 4L^2+4L^2 & -6L & 2L^2 & & \\ & & -12 & -6L & 12+12 & -6L+6L & -12 & 6L \\ & & 6L & 2L^2 & -6L+6L & 4L^2+4L^2 & -6L & 2L^2 \\ & & & & -12 & -6L & 12 & -6L \\ & & & & 6L & 2L^2 & -6L & 4L^2 \end{bmatrix} \begin{bmatrix} d_{y_1} \\ \phi_1 \\ d_{y_2} \\ \phi_2 \\ d_{y_3} \\ \phi_3 \\ d_{y_4} \\ \phi_4 \end{bmatrix}$$

$$\begin{bmatrix} F_{y_1} \\ m_1 \\ F_{y_2} \\ 0 \\ 0 \\ 0 \\ 160N \\ 0 \end{bmatrix} = \frac{EI}{L^3} \begin{bmatrix} 12 & 6L & -12 & 6L & & & & \\ 6L & 4L^2 & -6L & 2L^2 & & & & \\ -12 & -6L & 12+12 & -6L+6L & -12 & 6L & & \\ 6L & 2L^2 & -6L+6L & 4L^2+4L^2 & -6L & 2L^2 & & \\ & & -12 & -6L & 12+12 & -6L+6L & -12 & 6L \\ & & 6L & 2L^2 & -6L+6L & 4L^2+4L^2 & -6L & 2L^2 \\ & & & & -12 & -6L & 12 & -6L \\ & & & & 6L & 2L^2 & -6L & 4L^2 \end{bmatrix} \begin{bmatrix} 0 \\ 0 \\ 0 \\ \phi_2 \\ d_{y_3} \\ \phi_3 \\ d_{y_4} \\ \phi_4 \end{bmatrix}$$

$$\begin{bmatrix} 0 \\ 0 \\ 0 \\ 160N \\ 0 \end{bmatrix} = \frac{EI}{L^3} \begin{bmatrix} 4L^2+4L^2 & -6L & 2L^2 & & \\ -6L & 12+12 & -6L+6L & -12 & 6L \\ 2L^2 & -6L+6L & 4L^2+4L^2 & -6L & 2L^2 \\ & -12 & -6L & 12 & -6L \\ & 6L & 2L^2 & -6L & 4L^2 \end{bmatrix} \begin{bmatrix} \phi_2 \\ d_{y_3} \\ \phi_3 \\ d_{y_4} \\ \phi_4 \end{bmatrix}$$

$$\begin{bmatrix} \phi_2 \\ d_{y_3} \\ \phi_3 \\ d_{y_4} \\ \phi_4 \end{bmatrix} = \begin{bmatrix} 0.009\ rad \\ 0.001\ m \\ 0.0035\ rad \\ 0.003\ m \\ 0.0044\ rad \end{bmatrix} = \begin{bmatrix} 0.0508^o \\ 0.0047\ in \\ 0.203^o \\ 0.0130\ in \\ 0.2538^o \end{bmatrix} \tag{7}$$

The beam element calculations came very close to what Siemens NX had calculated, with only be one ten-thousandths of an inch off from each other. Therefore, the FEA from Siemens NX can be assumed to be correct.

iii) Von Misses Solution Keeping all of our previous assumptions and by observing that this structure is a cantilever beam, we are able to combine the equations for determining maximum stress of a cantilever beam in bending as well as under pure compressive forces. The result of this observation is the following equation:

$$\begin{aligned} \text{Stress} &= \text{Bending Stress} + \text{Compressive Stress} \\ \sigma &= \frac{12F_yL}{wh^2} + \frac{F_x}{wh} \\ \sigma &= \frac{12 * 35 * 2}{0.2 * 0.45^2} + \frac{200}{0.2 * 0.45} \\ \sigma &= 20,740psi + 450psi \\ \sigma &= 21,191psi \end{aligned} \tag{8}$$

This calculated Von Misses Stress agrees very well with our simulation with a discrepancy of only about 6%. In addition, the difference in stress from bending and compressive forces further validates our assumption that the beam component of the displacement will control the overall displacement. In other words, the off-axis displacement will be much greater than the on-axis displacement, despite the forces being heavily in favor of compressing the shank rather than bending it.

4.4 Wishbone Bracket

Main Contributer: Sam Purdy

4.4.1 Original Design

The chosen design for the overall project involves the weight being transferred from the wishbone to its bolt, and from that bolt to each of the two wishbone brackets. The original design for the wishbone bracket is shown below in figure 55.

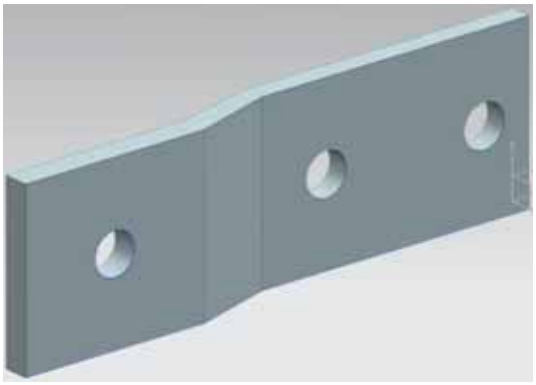

Figure 55: Original Design

This design was minimal, effective, and involves little effort to manufacture. Due to the importance of the piece however, it is desired for it to have as little displacement as possible, while still staying above or near our safety factor of 3. It needed to be able to survive cycles of axial loads, with the load concentrated to a single hole.

4.4.2 Finite Elemental Analysis

A basic FEA was performed on the piece, with a mesh size of 0.25 and Aluminum 6061 as the material, chosen due to its low density. The bottom hole was given a bearing load of 500 lbs and the other two holes were given pinned constraints, while the rear faces of the piece were fixed in the x direction, because of the way they will be mounted to each other and the wishbone. The maximum stress in the bracket reached 7176 psi with a displacement of 0.0082 in, giving the piece a safety factor of about 4.9. These are within the requirements we had set forth, however for the purposes of maximizing the capabilities of the system, we were able to produce several other

Iteration #	Design	Max Displacement (in)	Max Stress (psi)	Safety Factor
1	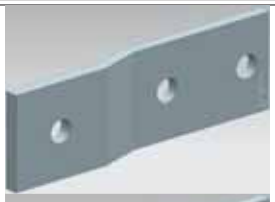	0.008163	7,176	4.88
2	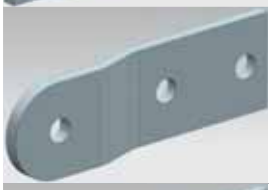	0.0101	8,163	4.29
3		0.006875	8,221	4.26
4		0.0094087	15,397	2.27
5		0.00053514	12,177	2.88

Table 3: Displacements and Stresses of Each Iteration Of Wishbone Bracket

designs that were tested with FEA as well. The results of each iteration, as well as a picture of each, is shown below in table 3.

While the Safety factor is lower in the final iteration than in the first, it is still near the desired safety factor and is far from failing. More importantly, the maximum displacement in the part was 0.0005 in, less than the original by more than a factor of 15. With much less of a range of motion every time the load is added and taken away, there is less fatigue on the part, and therefore its lifetime should increase. Detailed captures of the results of FEA on the final iteration are shown in Figure 56(a-b).

4.4.3 Verification

In order to confirm the validity of the results shown above, a basic hand calculation was performed, simplifying the system to be a two node 2D spring problem. This assumption should be relatively

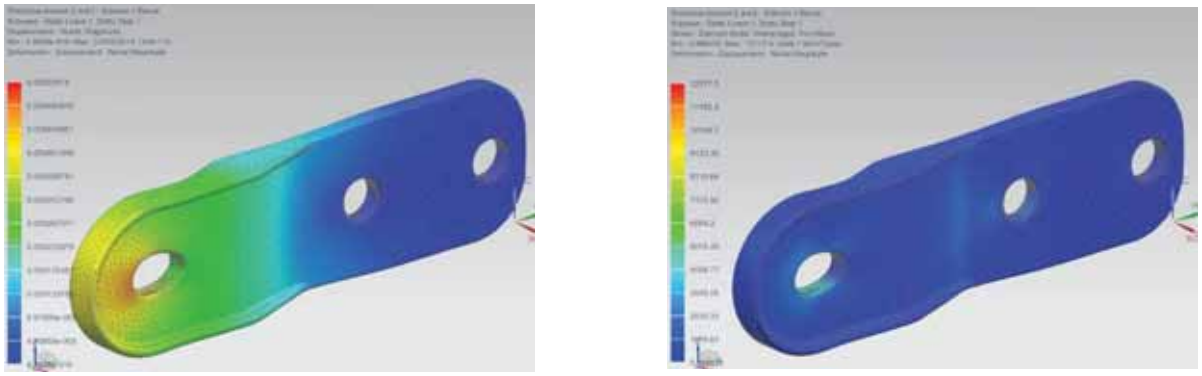

(a) Displacement (b) Von Misses Stress

Figure 56: Finite Elemental Analysis Results of Iteration #5

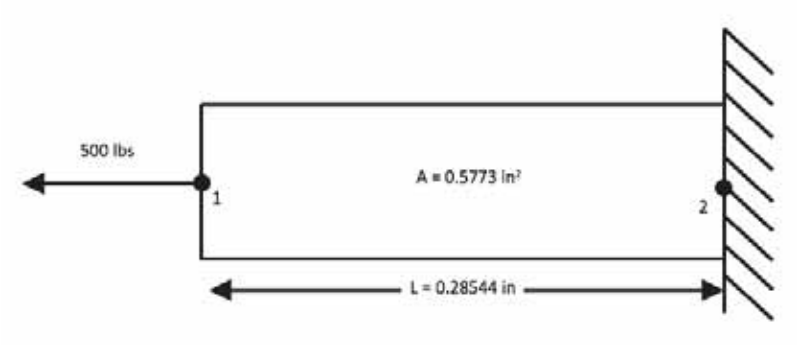

Figure 57: Simplified Layout for Hand Calculation

accurate due to the way the piece is mounted, with the top hole experiencing a negligible amount of deformation, the only two important areas are at the center of the middle and bottom holes. The problem layout is shown below in figure 57.

Approximating the distance between nodes one and two to have a constant cross sectional area equal to the average along the distance gives an area of about 0.5773 in2. Knowing the material used is Aluminum 6061, the Young's modulus is approximately 10004703 psi and the yield strength is 35056 psi. The following stiffness matrix was created using the properties shown.

$$k_{12} = \frac{AE}{L} \begin{bmatrix} F_1 = 500\ lbs \\ F_2 = react. \end{bmatrix} = \begin{bmatrix} k_{12} & -k_{12} \\ -k_{12} & k_{12} \end{bmatrix} * \begin{bmatrix} d_1 \\ d_2 = 0 \end{bmatrix} \tag{9}$$

After equating the answer to the above equations, the value of F_2 was calculated to be -500 lbs as expected. The value of d1 was also calculated to be 0.000247 in. As the computed value of max displacement was calculated to be 0.000535 in, the results of the hand calculation are not

far off, and so the results of the FEA can be stated as confirmed. Differences in the values can be attributed to the fact the object is not 2D and there is not a constant cross sectional area.

4.5 Hold Holder T-Bar

Main Contributer: Brandon Hagopian

4.5.1 Definitions

The base design for the T-Bar, the component that holds the slurried molds, consisted of Aluminum 6061, and was of very elementary design. The purpose of the following Finite Element Analysis for the T-Bar was to minimize its weight by iterating design changes to approach the best geometry. To simulate the weight of a slurried mold, a force of 60 pounds was applied to appropriate location, which is 20 inches extending along one arm of the T-Bar. This force is acting on the inside of the bolt hole, which is located inside the extrusion extending upward from the arm. The T-Bar mounts were fixed in 3 Dimensional Space, and a .2 inch 3D Tetrahedral mesh type was chosen.

4.5.2 Original Design

A maximum Von-Mises of stress of 171.17 psi occurred towards the cantilevered joint of the T-Bar. A maximum displacement of .0393 inches occurred at the outermost tip of the holder-arm, which is 22 inches long.

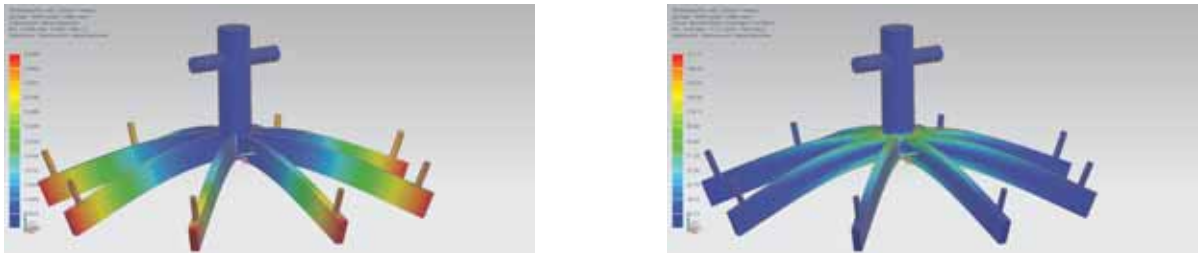

(a) Displacement (b) Von Misses Stress

Figure 58: Original T-Bar FEA

4.5.3 Verification

The original T-Bar was approximated to be a cantilevered beam. Six nodes were used to attempt to properly verify the maximum displacement. Refer to the following illustration demonstrating

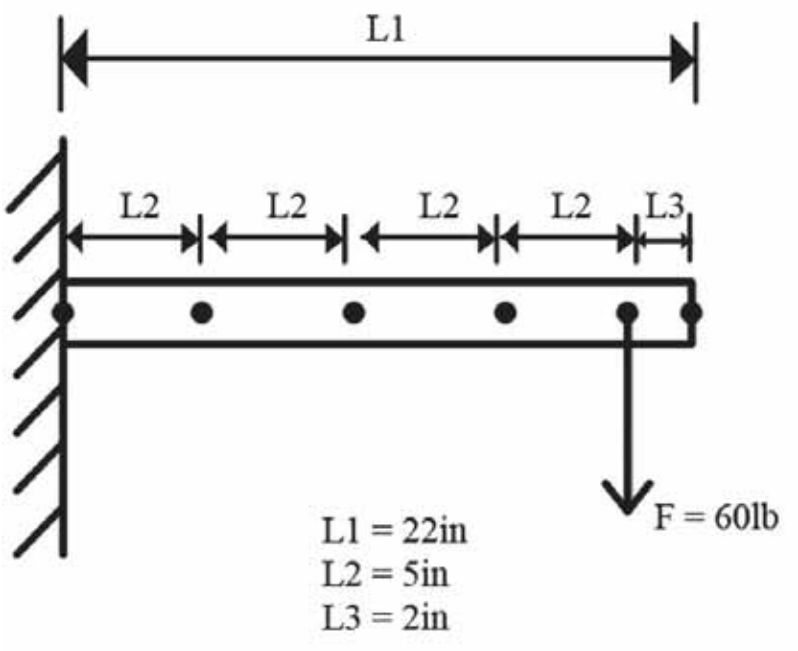

Figure 59: Illustration of Beam simplification

the approximation:

The 60 pound force is the weight of one slurried mold-tree. The following equivalent stiffness matrix was used in determining the unknown nodal displacements, angles, angles, and reaction forces and moments:

$$\begin{bmatrix} F_1 \\ m_1 \\ F_2 \\ m_2 \\ F_3 \\ m_3 \\ F_4 \\ m_4 \\ F_5 \\ m_5 \\ F_6 \\ m_6 \end{bmatrix} = EI \begin{bmatrix} \frac{12}{L_2^3} & \frac{6}{L_2^2} & \frac{-12}{L_2^3} & \frac{6}{L_2^2} & & & & & & & & \\ \frac{6}{L_2^2} & \frac{4}{L_2} & \frac{-6}{L_2^2} & \frac{2}{L_2} & & & & & & & & \\ \frac{-12}{L_2^3} & \frac{-6}{L_2^2} & \frac{24}{L_2^3} & 0 & \frac{-12}{L_2^3} & \frac{-6}{L_2^2} & & & & & & \\ \frac{6}{L_2^2} & \frac{2}{L_2} & 0 & \frac{8}{L_2^2} & \frac{-6}{L_2^2} & \frac{2}{L_2} & & & & & & \\ & & \frac{-12}{L_2^3} & \frac{-6}{L_2^2} & \frac{24}{L_2^3} & 0 & \frac{-12}{L_2^3} & \frac{6}{L_2^2} & & & & \\ & & \frac{6}{L_2^2} & \frac{2}{L_2} & 0 & \frac{8}{L_2} & \frac{-6}{L_2^2} & \frac{2}{L_2} & & & & \\ & & & & \frac{-12}{L_2^3} & \frac{-6}{L_2^2} & \frac{24}{L_2^3} & 0 & \frac{-12}{L_2^3} & \frac{6}{L_2^2} & & \\ & & & & \frac{6}{L_2^2} & \frac{2}{L_2} & 0 & \frac{8}{L_2} & \frac{-6}{L_2^2} & \frac{2}{L_2} & & \\ & & & & & & \frac{-12}{L_2^3} & \frac{-6}{L_2^2} & 12(\frac{1}{L_2^3}+\frac{1}{L_3^3}) & 6(\frac{1}{L_3^3}-\frac{1}{L_2^3}) & \frac{-12}{L_3^3} & \frac{6}{L_3^2} \\ & & & & & & \frac{6}{L_3^2} & \frac{2}{L_3} & 6(\frac{1}{L_3^3}-\frac{1}{L_2^3}) & 4(\frac{1}{L_2}+\frac{1}{L_3}) & \frac{-6}{L_3^2} & \frac{2}{L_3} \\ & & & & & & & & \frac{-12}{L_3^3} & \frac{-6}{L_3^2} & \frac{12}{L_3^3} & \frac{-6}{L_3^2} \\ & & & & & & & & \frac{6}{L_3^2} & \frac{2}{L_3} & \frac{-6}{L_3^2} & \frac{4}{L_3} \end{bmatrix} \begin{bmatrix} d_1 \\ \theta_1 \\ d_2 \\ \theta_2 \\ d_3 \\ \theta_3 \\ d_4 \\ \theta_4 \\ d_5 \\ \theta_5 \\ d_6 \\ \theta_6 \end{bmatrix} \tag{10}$$

Solving this equation provides the following results:

$$\begin{bmatrix} F_1 \\ M_1 \\ d_2 \\ \theta_2 \\ d_3 \\ \theta_3 \\ d_4 \\ \theta_4 \\ d_5 \\ \theta_5 \\ d_6 \\ \theta_6 \end{bmatrix} = \begin{bmatrix} 60 \\ 1200 \\ 0.00061 \\ 0.00023 \\ 0.00222 \\ 0.00040 \\ 0.00450 \\ 0.00050 \\ 0.00711 \\ 0.00053 \\ 0.00817 \\ 0.00053 \end{bmatrix} \tag{11}$$

The maximum displacement provided by NX Nastran, Linear Statics, was approximately .0393 inches. The maximum displacement provided by the hand calculation was .00817 inches. This

difference as a percentage is equal to 20.78%. The reason for this difference is likely the use of a different Elastic Modulus in the NX simulation than the hand simulation. Also, the type of mesh used was a 3D Tetrahedral mesh, .2 inches in size—while the hand calculation used a mesh size of 5 inches in length, and 1 inches in thickness.

4.5.4 Iteration #8

The following simulation and hand calculation is of the eighth iteration of design of the T-Bar:

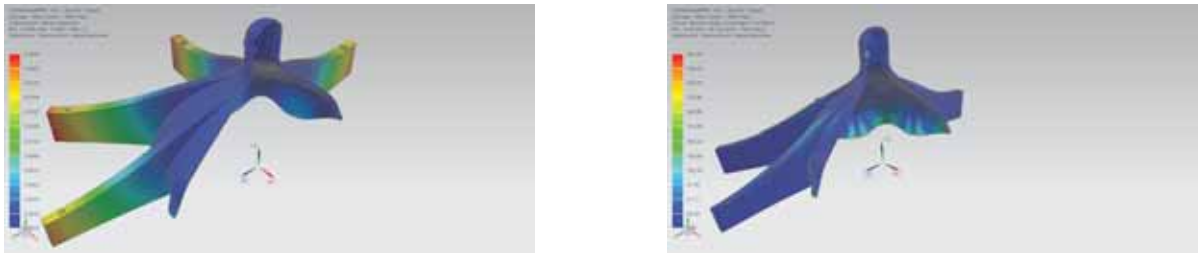

(a) Displacement (b) Von Misses Stress

Figure 60: Iterated T-Bar FEA

Using the same constraints and applied forces as the original T-Bar design, the maximum displacement of any node on the structure was .0220 inches, according to NX Nastran Solver—Linear Statics. This maximum displacement occurred in an intuitive location, which was at the very end of the arm. The hollow cavity of this particular iteration showed signs of inward deformation, which later on, will be compensated for through the last iterations of design. The maximum Von-Mises Stress was 367.02 psi, which occurred at the holding mount. Before the design process continued, an FEA hand calculation was performed on this particular geometry, of iteration 8.

4.5.5 Verification

In order to attempt a proper hand calculation of this particular complex geometry, simplifications of great magnitude had to be made. The following diagram shows the simplification of the 8th iteration of the T-Bar:

This simplification was split into two parts: a variable cross-sections cantilever and a variable cross-sectioned beam in tension. The 60lbf was split into a perpendicular component acting on the end of the beam and a tangent force acting along the beam's axis in tension.

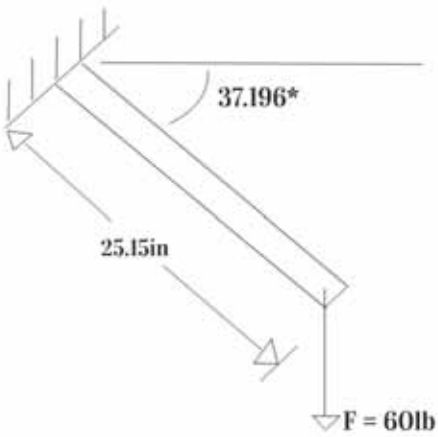

Figure 61: Simplified FEA Calculation

$$F_{Tensile} = F\sin(37.196) = 36.27\ lbf$$
$$F_{Perpendicular} = F\cos(37.196) = 47.79\ lbf \tag{12}$$

(a) Tensile Component of Load (b) Cantilevered Portion of Load

Figure 62: Simplified FEA Loads in their Components

These two individual beams are solved for the maximum displacement using the following equations:

Tensile Member Load:

$$\text{Elastic Modulus of ABS Plastic} = 29,0075\ psi$$

$$\text{Area of First Cross Section} = 36\ \frac{lb}{in^2}$$

$$L = \text{Distance Between Each Node} = 6.2863\ in$$

$$\text{Area of Second Cross Section} = 2.4\ in^2$$

$$k_1 = \frac{A_1 * E}{L} = \text{Spring Constant}$$
$$k_2 = \frac{A_2 * E}{L} = \text{Spring Constant}$$

$$\begin{bmatrix} f_1 \\ f_2 \\ f_3 \\ f_4 \\ f_5 \end{bmatrix} = \begin{bmatrix} k_1 & -k_1 & & & \\ -k_1 & 2k_1 & -k_1 & & \\ & -k_1 & k_1+k_2 & -k_2 & \\ & & -k_2 & 2k_2 & -k_2 \\ & & & -k_2 & k_2 \end{bmatrix} \begin{bmatrix} d_1 \\ d_2 \\ d_3 \\ d_4 \\ d_5 \end{bmatrix} \tag{13}$$

$$\begin{bmatrix} f_1 \\ d_2 \\ d_3 \\ d_4 \\ d_5 \end{bmatrix} = \begin{bmatrix} -36.27 \\ 2.18E-5 \\ 4.36E-5 \\ 3.71E-4 \\ 6.98E-4 \end{bmatrix} \tag{14}$$

Cantilevered Load:

$$Constant_1 = E * I_1 = C_1$$

$$Constant_2 = E * I_2 = C_2$$

$$ElasticModulusforABSPlastic = 290075.48psi$$

$$\begin{bmatrix} f_1 \\ m_1 \\ f_2 \\ m_2 \\ f_3 \\ m_3 \\ f_4 \\ m_4 \\ f_5 \\ m_5 \end{bmatrix} = \begin{bmatrix} 12C_1(l^-3) & 6C_1(l^-2) & -12C_1(l^-3) & 6C_1(l^-2) & & & & & & & & & & \\ 6C_1(l^-2) & 4C_1(l^-1) & 6C_1(l^-2) & 2C_1(l^-1) & & & & & & & & & & \\ -12C_1(l^-3) & -6C_1(l^-2) & 24C_1(l^-3) & 0 & & & & & & & & & & \\ 6C_1(l^-2) & 4C_1(l^-1) & 6C_1(l^-2) & 2C_1(l^-1) & -12C_1(l^-3) & -6C_1(l^-2) & & & & & & & & \\ & & -12C_1(l^-3) & -6C_1(l^-2) & 12(l^-3)(C_1+C_2) & 6(l^-2)(C_2-C_1) & 12C_2(l^-3) & -6C_2(l^-2) & & & & & & \\ & & 6C_1(l^-2) & 2C_1(l^-1) & 6(l^-2)(C_2-C_1) & 4(l^-1)(C_1+C_2) & -6C_2(l^-2) & 2C_2(l^-1) & & & & & & \\ & & & & -12C_2(l^-3) & -6C_2(l^-2) & 24C_2(l^-3) & 0 & 12C_2(l^-3) & -6C_2(l^-2) & & & & \\ & & & & 6C_2(l^-2) & 2C_2(l^-1) & 0 & 8C_2(l^-1) & -6C_2(l^-2) & 2C_2(l^-1) & & & & \\ & & & & & & -12C_2(l^-3) & -6C_2(l^-2) & 24C_2(l^-3) & 0 & 12C_2(l^-3) & -6C_2(l^-2) & & \\ & & & & & & -6C_2(l^-2) & 2C_2(l^-1) & -6C_2(l^-2) & 4C_2(l^-1) & & & & \end{bmatrix} \begin{bmatrix} d \\ \\ d \\ \\ d \\ \\ d \\ \\ d \\ \\ \end{bmatrix} \tag{15}$$

$$\begin{bmatrix} f_1 \\ m_1 \\ d_{2_y} \\ \theta_2 \\ d_{3_y} \\ \theta_3 \\ d_{4_y} \\ \theta_4 \\ d_{5_y} \\ \theta_5 \end{bmatrix} = \begin{bmatrix} -47.48 \\ 156.06 \\ -.0077 \\ -.0029 \\ -.0432 \\ -.0087 \\ -.0045 \\ -.0225 \\ -.1975 \\ -.0374 \end{bmatrix} \tag{16}$$

The maximum displacement of the cantilevered beam is approximately equal to -.1975 inches.

Using these two maximum displacement values of -.1975 and .000698 inches, the magnitude of the displacement can be calculated as follows:

$$c^2 = a^2 + b^2 \fallingdotseq .1975\ in$$

The NX Nastran solver produced a maximum displacement of the end of the beam to be .022 inches. This difference can be attributed the crude approximation technique of finding the vector magnitude of the displacements of the T-Bar split into two different scenarios.

4.5.6 T-Bar Further Optimizations

Because of the deformation pattern of Iteration 8, mentioned previously, an interior structural geometry was added to combat the deformation pattern. This interior geometry is shown in the

following image:

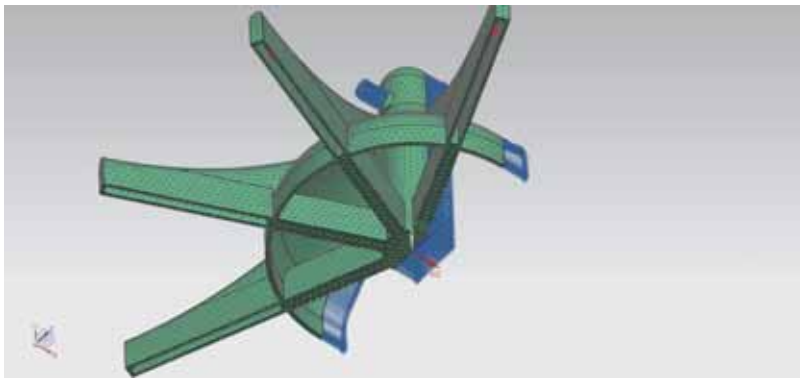

Figure 63: Interior Geometry Change

After this interior geometry was combined with the original hollowed T-Bar, another FEA analysis was attempted:

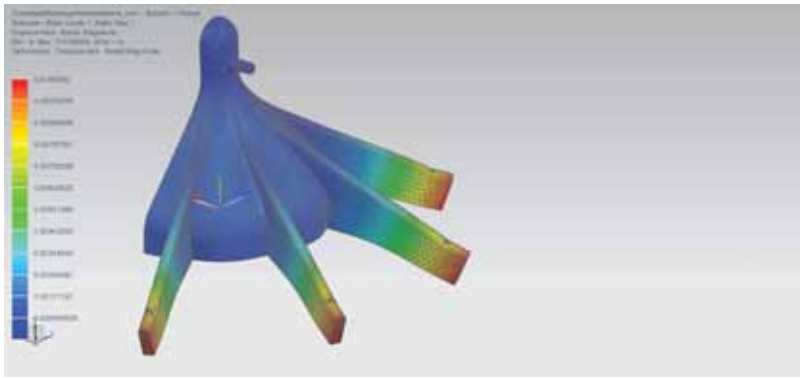

Figure 64: Displacement

Shown in the image, the stresses were transferred to the mount extruded from the part. The maximum Von-Mises stress is equal to 333.10 psi, while the maximum deformation was .008in. This value of .008in is a stark improvement from the previous value of .0220 inches.

4.5.7 Verification

The maximum stress is in either shear mode or bending mode, and can be approximated by a simple cantilevered beam with a distributed load acting on the length of the mount. A simplified diagram is shown here:

Figure 65: Von Misses Stress

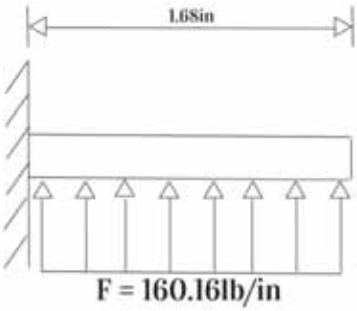

Figure 66: Simplified System

$$\text{Density of ABS Plastic} = .054\ \frac{lb}{in^3}$$

$$\text{Volume of Half of T-Bar} = 538.54\ in^3$$

$$F = \text{Density ABS} * \text{Volume Half of T-Bar} + 4\text{Molds} * 60\frac{lbf}{\text{Mold}} = 269.08\ lbf$$

$$\text{Maximum Shear Stress} = \frac{269.08}{\text{Area Cross Section}} = 485.54\ psi$$

$$\text{Maximum Bending Stress} = \frac{Mc}{I} = 685.2\ psi$$

Through a simple hand calculation, the concentrated force of 269.08lbf acts at the center of the beam, producing a shear stress of 485.54 psi. The maximum bending stress is not to be considered any further in this analysis due to the particular constraints of the T-Bar geometry

with respect to its parent component in the full assembly. The Maximum Shear Stress calculated by hand is 31.39% different than the NX Nastran Solver value of 333.1 psi. The reason for this difference is the simplified geometry of the hand calculation. The mount on the actual T-Bar consists of a smoothed edge, while the hand calculation does not take this into account. This result agrees intuitively due to the phenomenon of the reduction of a stress concentration with smoother curvatures, shown in the following figure:

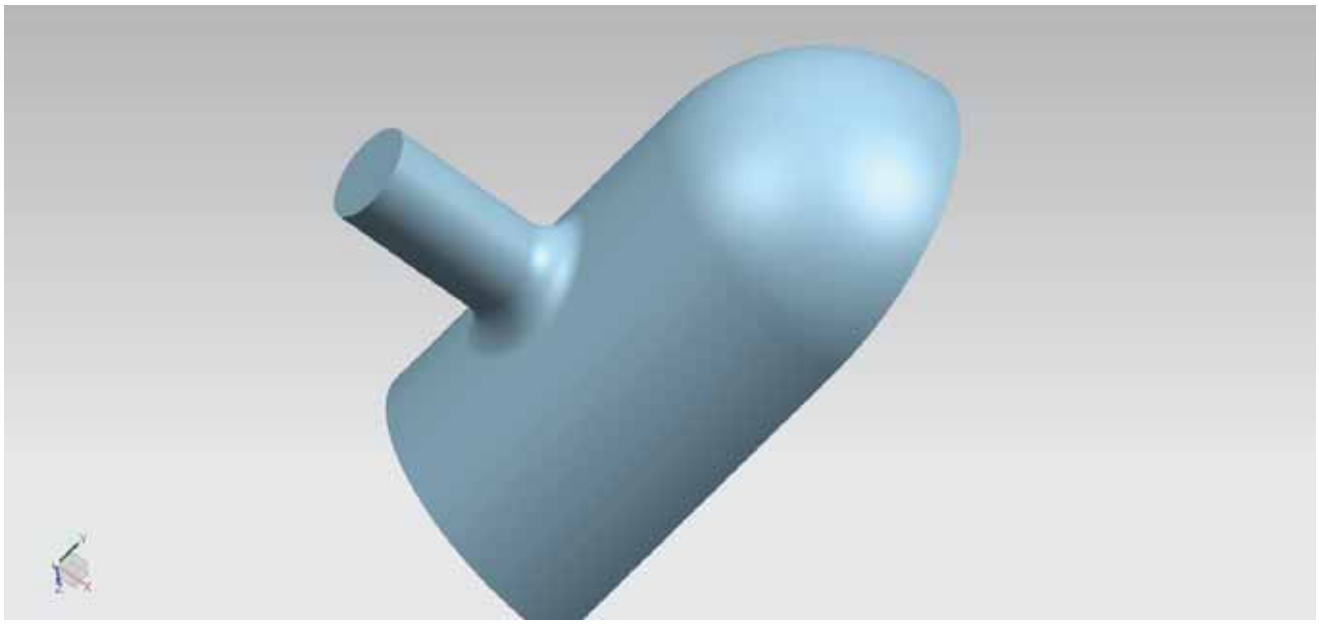

Figure 67: Edge Blend

5 Summary

In this project, imperfections of an existing design were identified, analyzed, and corrected through an iterative design process. This design process was spearheaded by Siemens NX FEA simulations and later verified to be accurate by simplified hand calculations. through Siemens NX, stress concentrations were easy to identify and correct. It allowed faster iteration than what hand calculations alone would allow.

Overall, we developed a system to more accurately locate molds in 3D space to allow for less error prone automated manufacturing processes. This system was inspired by the existing technology in ski-lift support towers. By having a pivoting roller bar, the point of contact of profiled rollers would be varied, starting from the point of most locational certainty and moving to the point of least locational certainty. Due to the constant spring force, provided by a sealed air cylinder in the locating bracket assembly, the roller would never be lifted away from the wishbone, ensuring the point of least locational certainty is properly restrained. A method of weighing the products was also added in such a way to not interfere or increasing the time of the value-adding robotic processes. This was achieved by measuring the force it takes to rotate the mold a certain number of degrees. A simple force analysis will see that the force exerted on a horizontal force transducer is directly proportional to the mold weight.

Despite improving upon the industry standard design, we also optimized our own design by performing FEA on several key components and ensuring every component in our design has a Factor of Safety of around 3, but no more than 10. We want to avoid excess material wherever possible, but still have a long lasting product. These components include the pin from which the hanger is suspended from, the mold plate which holds several molds together as one assembly, the frame which the suspended conveyor system is suspended from, and the shank of piston taking the weight measurement through a force transducer.

6 Future Work

One of the main points of improvement is to make a stand-alone system. This would include the chain drive motor, chain tensioner, and the shutter to separate the rooms. This would effectively create a single marketable product. To put this in the form of an analogy, we would go from producing only the transmission of a car to producing the entire car. The entire car would be easier to market and has a greater potential for success, if that initial effort of designing the entire car is invested.

Additionally, the drive motor design has a great degree of potential cleverness. the minimal viable design would simply be a Pulse Width Modulated (PWM) motor geared down to drive large gears, which mesh into the chain drive. However, there is a great amount of potential improvements that can be made. Say we adopt the car analogy again, this large gear is akin to the transmission of a car, connecting the power (PWM Motor) to the drive (Chain Drive). With this, we could borrow some of the technological improvements found in modern day clutches, such as the internal, tangentially-orientated coil springs that deaden jerk. The immediate benefit would be a reduction in the mold jerk. Not only would that make the drying of the molds more consistent, but it would also reduce dangerous rocking of the molds and prevent collisions.

To add to this thought, the belt tensioner and drive motor could talk to each other. Take the situation that the drive motor controller is sensing current oscillations, which indicate rocking because the motor, operating at a constant rotation, will try harder to correct a backwards rocking and have to try less for the mold rocking forwards, the tensioner could relieve tension on the chain. This relieving of the tension would allow the rocking energy would be dissipated harmlessly through friction due to the slackness of the chain. Once the current oscillations are under a certain threshold, the tension could be restored gradually. A PID controller would be ideal in this scenario.

To expand the data collecting aspect of this project further, a plethora of add-ons could be offered for the client to pick and choose what locating and data packages they want. A standardized mounting plate could be devised of which any number of force transducers, induction sensors, RFID readers, or image processing cameras could be attached with only custom-made brackets to angle these devices to the customer's specification. This design philosophy would allow the flexibility to

adapt the system to any customer's industry specific requirements while minimizing the work on the main structure of the system.